Interhemispheric SST gradient trends in the Indian Ocean prior to and during the recent global warming hiatus

Lu Dong[1*], Michael J. McPhaden[1]

1 NOAA/PMEL, Seattle, Washington, USA

Revision submitted to *J. Climate*

July 7, 2016

<u>Corresponding author:</u>

Lu Dong

NOAA/Pacific Marine Environmental Laboratory

7600 Sand Point Way NE, Seattle, Washington, USA 98115

E-mail: lu.dong@noaa.gov

Abstract

Sea surface temperatures (SSTs) have been rising for decades in the Indian Ocean in response to greenhouse gas forcing. However, in this study we show that during the recent hiatus in global warming, a striking interhemispheric gradient in Indian Ocean SST trends developed around 2000, with relatively weak or little warming to the north of 10°S and accelerated warming to the south of 10^{o}S. We present evidence from a wide variety of data sources that this interhemispheric gradient in SST trends is forced primarily by an increase of Indonesian Throughflow (ITF) transport from the Pacific into the Indian Ocean induced by stronger Pacific trade winds. This increased transport led to a depression of the thermocline that facilitated SST warming presumably through a reduction in the vertical turbulent transport of heat in the southern Indian Ocean. Surface wind changes in the Indian Ocean linked to the enhanced Walker circulation also may have contributed to thermocline depth variations and associated SST changes, with downwelling favorable wind stress curls between 10^{o}S and 20^{o}S and upwelling favorable wind stress curls between the equator and 10^{o}S. In addition, the anomalous southwesterly wind stresses off the coast of Somalia favored intensified coastal upwelling and off-shore advection of upwelled water, which would have led to reduced warming of the northern Indian Ocean. Though highly uncertain, lateral heat advection associated with the ITF and surface heat fluxes may also have played a role in forming the interhemispheric SST gradient change.

1. Introduction

The Indian Ocean has witnessed a significant sea surface temperature (SST) warming trend during the twentieth century (Alory et al. 2007; Du and Xie 2008), which has been broadly attributed to increased anthropogenic greenhouse gas (GHG) emissions into the atmosphere (Dong et al. 2014; Dong and Zhou 2014). Superimposed on the pronounced warming trend, Indian Ocean SST also exhibits considerable natural decadal variability (Lee and McPhaden 2008; Trenary and Han 2013; Nidheesh et al. 2013; Han et al. 2014; Dong et al. 2016). Many studies have demonstrated how a modified Walker circulation can affect Indian Ocean SSTs during ENSO events (e.g. Yu et al. 1999; Alexander et al. 2002; Schott et al. 2009). More recently, a remote influence of the Pacific Ocean on Indian Ocean decadal variability through both the atmosphere and the ocean has also been identified (Reason et al. 1996; Cai et al. 2008; Lee and McPhaden 2008; Trenary and Han 2013; Dong et al. 2016). The oceanic route is linked to transports through the Indonesian Archipelago that can influence upper-ocean heat content and sea level in the tropical southern Indian Ocean (Schwarzkopf and Böning 2011; Feng et al. 2011). For example, a basin-wide warming/cooling pattern dominates Indian Ocean SST decadal variability (Han et al. 2014), modulated by Pacific Decadal Oscillation (PDO)-induced atmospheric adjustment through changing surface heat fluxes, sea surface height and thermocline depth (Dong et al. 2016). There has also been a significant decadal change in sea level variability in the Indian Ocean around 2000, affected by both local wind stress variations and remote forcing from the western Pacific (Lee and McPhaden 2008; Han et al. 2010; Feng et al. 2010; Li and Han 2015).

In addition to these variations, global surface warming from the start of twenty-first century to 2013 largely stalled despite the ongoing increase in atmospheric GHG concentrations (e.g. Easterling and Wehner 2009; Meehl et al. 2011; Kosaka and Xie 2013; England et al. 2014). A number of scientific hypotheses have been put forward to explain the hiatus, although the reasons behind it are still debated. Anomalously cold La Niña-like SSTs in the eastern Pacific associated with the negative phase PDO have been identified as a key component to the hiatus in global mean surface temperature rise (Meehl et al. 2011; Kosaka and Xie 2013). Lee et al. (2015) and Nieves et al. (2015) have demonstrated the role of the Indonesian Throughflow (ITF) into Indian Ocean, driven by enhanced trades associated with the negative phase PDO, in regulating the oceanic heat budget during the recent hiatus. A global ocean general circulation model (OGCM) reveals that blockage of the ITF can raise the mean thermocline and decrease SST in the southern Indian Ocean (Lee et al. 2002), while enhanced ITF transport will deepen the thermocline and lead to elevated SSTs in the southern Indian Ocean (Hirst and Godfrey 1993).

During the second half of twentieth century, ocean heat content in the Indian Ocean increased, but the increase was not spatially uniform. In particular, there was an evident hemispheric asymmetry, with a slower accumulation of heat in the northern Indian Ocean than in the southern Indian Ocean (Levitus et al. 2012; Han et al. 2014). Attempts have been made to explain this hemispheric asymmetry in terms of anthropogenic forcing, especially higher aerosol concentrations, in causing the slower rate of warming in the Northern Hemisphere (Barnett et al. 2005; Pierce et al. 2006). Chung and Ramanathan (2006) also argued that reduced solar radiation from South Asian aerosols accounted for a reduced rate of SST warming in the northern Indian Ocean since the 1950s. D'Mello and Kumar (2015) suggested that the increasing prevalence of depressions, cyclones and severe cyclones is another possible reason for the reduced rate of SST warming in Bay of Bengal after 1995. In contrast, Roxy et al. (2016) identified a SST warming trend in the northwestern Indian Ocean during 1998-2013, associated with enhanced ocean stratification and a reduction the phytoplankton abundance. Most of the above studies used only one SST product in their analysis. In connecting our results to these previous studies, we will use several SST products to address the robustness of the observed trends.

SST variations in the Indian Ocean have large impacts on rainfall and atmospheric circulation in the region, especially Africa and South Asia (Hoerling et al. 2004; Krishnan et al. 2006; Zhou et al. 2009; Lyon and DeWitt 2012; Roxy et al. 2015). In this study, we focus on a previously unexplored aspect of SST variability in the Indian Ocean spanning the recent global warming hiatus and the preceding pre-hiatus decade, namely a striking interhemispheric gradient in SST trends that has developed since about 2000. As we shall see, SST warming plateaued in the northern Indian Ocean after 2000, while an enhanced warming SST occurred in the southern Indian Ocean during the same period (Fig. 1). We aim to clarify the characteristics of this interhemispheric trend and highlight the mechanisms responsible for it. In particular, we will elaborate on the potential role of the Pacific Ocean in driving changes in Indian Ocean winds and ITF transports to form this interhemispheric gradient. We present evidence that the interhemispheric gradient in the Indian Ocean SST trend is forced by an increase of ITF transport from Pacific to Indian Ocean and the wind stress changes associated with the Pacific circulation. Though the enhanced ITF transport and changes in the Walker circulation during recent decades have been described in many previous studies (e.g. Luo et al. 2012; Sohn et al. 2013; England et al. 2014; Lee et al. 2015; Nieves et al. 2015), their contributions in forming the interhemispheric gradient changes in the Indian Ocean SSTs between the pre-hiatus and recent hiatus periods is a novel aspect of our study. We also find that, though highly uncertain, increased latent heat loss from the ocean would also favor a relative cooling of SST in the northern Indian Ocean.

The remainder of the paper is organized as follows. The data and analysis methods are described in section 2. In section 3, we identify the interhemispheric gradient trends in Indian

Ocean SST during the recent hiatus compared to the pre-hiatus decade. Then we investigate the contributions of decadal changes in ITF transport and related variations in thermocline depth, as well as the roles in large-scale Pacific trade winds and related Indian Ocean wind stress variations. Finally, the role of surface heat fluxes and ITF-induced lateral heat advection are estimated. We conclude with a summary and discussion in section 4.

2. Data and analysis methods

a. Data description

Six different monthly SST data sets are used: (1) Hadley Centre Global Sea Ice and Sea Surface Temperature (HadISST: 1° latitude × 1° longitude; Rayner et al. 2003); (2) Kaplan Extended SST version 2 (Kaplan_V2: 5° latitude × 5° longitude; Kaplan et al. 1998); (3) National Oceanic and Atmospheric Administration Extended Reconstructed SST version 3 (ERSST_v3b: 2° latitude × 2° longitude; Smith et al. 2008); (4) Hadley Centre SST version 3 (HadSST3: 5° latitude × 5° longitude; Kennedy et al. 2011a, b); (5) NOAA Optimum Interpolation SST version 2 (OISST_V2: 1° latitude × 1° longitude; Reynolds et al. 2002); (6) TropFlux, with spatial resolution of 1° latitude × 1° longitude covering the entire 30°N-30°S region (Kumar et al. 2012).

Changes in observed upper ocean temperature are estimated using objectively analyzed monthly climatological ocean temperature fields from the World Ocean Atlas (WOA: 1° latitude × 1° longitude; Levitus et al. 2012) and seasonal fields from World Ocean Database 2009 (WOD: 1° latitude × 1° longitude; Boyer et al. 2009), monthly variations from the Ishii data base (1° latitude × 1° longitude; Ishii et al. 2005) and monthly variations from the EN4 objective analysis dataset (1° latitude × 1° longitude; Good et al. 2013). We compare these observations with temperature fields from monthly ocean reanalysis products using (1) NCEP Global Ocean Data Assimilation System (GODAS: 1/3° latitude × 1° longitude; Nishida et al. 2011); (2) the latest

European Centre for Medium Range Weather Forecasts ocean reanalysis system 3 and 4 (ORA-S3: 1.4° to 0.3° increases gradually toward the equator latitude × 1.4° longitude; ORA-S4: 1° latitude × 1° longitude; Balmaseda et al. 2008, 2013); (3) the Simple Ocean Data Assimilation version 2.2.4 (SODA2.2.4: 0.5° latitude × 0.5° longitude; Carton and Giese 2008); (4) the second German contribution to Estimating the Circulation and Climate of the Ocean system (GECCO2: 1° latitude × 1° longitude; Köhl 2015).

For wind stress fields, we use monthly 20CRv2 (Giese and Ray 2011) that is used to force SODA2.2.4 (0.5° latitude × 0.5° longitude; Carton and Giese 2008), TropFlux (1° latitude × 1° longitude for 30°N-30°S; Kumar et al. 2012), and European Centre for Medium-range Weather Forecasts Re-Analysis (ERA)-Interim (0.75° latitude × 0.75° longitude; Dee et al. 2011). For surface heat flux fields, we use monthly outputs from TropFlux, ERA-Interim, the Objectively Analyzed Air-Sea Fluxes (OAFlux: 1° latitude × 1° longitude; Yu et al. 2008), and National Centers for Environmental Prediction–Department of Energy (NCEP2: 1.9° latitude × 1.875° longitude; Kanamitsu et al. 2002). For horizontal ocean current, we use monthly outputs from SODA2.2.4, GECCO2, ORA-S3, and ORA-S4.

Daily ITF transport data from the International Nusantara Stratification and Transport (INSTANT) program (Sprintall et al. 2009) are used for comparison with the ocean analyses covering the 3-year period 2004-2006. The INSTANT data span the full depth range in the three main passages for ITF transport, namely the Lombok Strait, the Ombai Strait, and Timor Passage. The observed monthly PDO index, derived as the leading principal component of monthly SST anomalies in the North Pacific Ocean poleward of 20°N is available from http://research.jisao.washington.edu/pdo/PDO.latest.

b. Analysis methods

We consider decadal changes during the transition from the pre-hiatus period (1984-1999) to the recent hiatus period (2000-2013), a time span covered by all the data sets described above. These periods are chosen based on the assumption that the hiatus began in approximately 2000. It is known that computing trends from short record segments is sensitive to the choice of start and end points. Also, there is significant year-to-year variability in the annual mean SSTs in the Indian Ocean (Fig. 1), some of which is related to El Niño/Southern Oscillation (ENSO) and the Indian Ocean Dipole (IOD) fluctuations. However, choosing a different transition year between the two periods of interest in our study does not qualitatively affect our basic conclusions. For example, the overlapping 15-year SST trend shows that the interhemispheric gradient changed from positive to negative around 2000 (Fig. 2). It is indicated that the period 1997-2001, affected by a major swing in the ENSO cycle, does not change the result significantly. Thus the results presented here are robust (i.e., qualitatively insensitive to the details of how we define the transition). We also note the negative gradient in interhemispheric trends that developed since 2000 is not unique in the climate record and there is a stronger one that occurred during 1970s. However, considering that most products (such as OISST_V2, TropFlux, GODAS, NCEP2, ERA-Interim, OAFlux) used here do not cover the period before 1970s, we only focus on the recent hiatus and pre-hiatus decade in this study.

Note that for the purposes of this study, we define the northern and southern hemispheres in the Indian Ocean with a dividing line at 10^{o}S rather than at the geographic equator. This boundary is chosen based for the following reasons: (1) it is the hemispheric boundary of the SST changes that we will describe below (Figs. 3-5); (2) it is along the southern edge of the warm pool in the central-eastern Indian Ocean characterized by SST greater than 28^{o}C (Fig. 5); (3) it is near the latitude where surface winds transit from trade wind to monsoonal regimes. South of about

10°S, the southeast trades are relatively steady around the year, while north of 10°S the winds vary markedly, reversing direction with the season (Schott et al. 2009); (4) the Indian Oceans south of 10°S is most directly affected by the ITF (Hirst and Godfrey 1993; Lee et al. 2002). Following this definition, the ocean area of northern Indian Ocean covering 30°N-10°S ($2.3*10^7$ km^2) and southern Indian Ocean covering 10°S-40°S ($2.5*10^7$ km^2) are comparable (Figs. 3-5). Significance levels for the decadal variations we show represent 95% confidence limits based on a two sided Student t-test.

Thermocline depth is defined as the depth of the 20°C isotherm, which is located in the middle of the thermocline. The ITF transport in the ocean reanalysis products is usually computed as the total-depth vertically integrated velocity through the IX1 eXpendable BathyThermograph (XBT) line (6.8°S, 105.2°E-31.7°S, 114.9°E) (Wijffels and Meyers 2003). To simplify the calculation, we choose the nearest straight north-south line (8°-25°S along 113°E) instead of the XBT line. The results are reliable by comparing with the INSTANT data and previous studies. The transport across this line integrates flow coming into Indian Ocean through the three major exit passages of the Lombok Strait, Ombai Strait, and Timor Passage.

3. Results

a. Interhemispheric gradient trends in Indian Ocean SST during the recent hiatus compared to the previous decade

To examine the Indian Ocean SST changes in each hemisphere, we start by comparing the time evolution of the northern and southern Indian Ocean SST from different observational data sets (Fig. 1). A significant warming trend is seen during 1950–2014, with similar magnitudes of 0.11 °C per decade in both southern and northern Indian Ocean. This long-term trend mainly results from GHG forcing (Dong and Zhou 2014). Embedded within the long-term trend, decadal variations are also present; in particular, there is a significant decadal change in the interhemispheric SST gradient around the start of global warming hiatus in 2000. During the pre-hiatus decade (1984-1999), the warming trend in northern Indian Ocean is stronger than in southern Indian Ocean. In contrast, during the recent hiatus decade (2000-2013), the warming in northern Indian Ocean stalled but that in southern Indian Ocean continued and even increased (Fig. 1c, d). Thus, a significant interhemispheric gradient in SST trends appears in the Indian Ocean during the recent global warming hiatus, which has not been described in previous studies.

Next we consider the spatial distribution of the decadal changes in the SST trends during the recent hiatus decade compared with a pre-hiatus warming decade (Figs. 3-5). During pre-hiatus decade (1984-1999), warming trends cover the northern Indian Ocean including along the Somalia coast as pointed out by Roxy et al (2016), while weak cooling trends are evident in the southern Indian Ocean (Fig. 3). In contrast, during the recent hiatus (2000-2013), warming trends in the southern Indian Ocean become much stronger than those in the north (Fig. 4). Specifically, the warming in the northwestern Indian Ocean is consistent with Roxy et al. (2016), but with smaller magnitude compared to pre-hiatus decade. Thus, the trend difference between the two periods is negative in this region (Fig. 5). We also see a reduced warming rate in Bay of Bengal during the recent hiatus decade compared to the pre-hiatus decade, consistent with the results of D'Mello and Kumar (2015). Thus, SST warming trends become weaker during the recent hiatus than pre-hiatus decade in the northern Indian Ocean and stronger in the southern Indian Ocean, with a boundary located along the 10ºS (Fig. 5).

Decadal changes of mean thermocline depth (Fig. 6) indicate that the thermocline deepened significantly in the hiatus decade compared to the pre-hiatus decade in the southern Indian Ocean, consistent across all eight ocean reanalysis products. For the northern Indian Ocean, the changes are generally less robust, though several data sets and the eight-product average show a tendency for a shoaling thermocline, especially along the Somalia coast. A deeper thermocline can limit the effectiveness of vertical mixing to cool the surface, and vice versa for a shallower thermocline (Lee et al. 2002). Thus, we infer that the observed decadal changes of thermocline depth favor the decadal changes in interhemispheric SSTs, a point we elaborate on further next.

To highlight the contribution of thermocline depth changes to the observed decadal change in interhemispheric SST gradient, we compare the 15-year running trend of SST and thermocline depth averaged in the southern Indian Ocean. Both show an increasing positive trend during the recent hiatus decade compared to the pre-hiatus decade (Figs. 7a, b). Then we regressed the SST running trend onto the thermocline depth running trend, and multiplied the regression pattern with the decadal changes of thermocline depth trends between the hiatus decade and pre-hiatus decade at each grid point. This procedure provides an estimate of how changes in thermocline depth contribute to changes in SST trends (Fig. 7c). For the average of southern Indian Ocean, the observed increase of SST warming trend between the two periods is 0.11±0.03 ºC decade^{-1} based on 6 products we used (error bounds are for 95% confidence limits). The changes of thermocline depth have a positive contribution of 0.08±0.006 ºC decade^{-1}, indicating that more than 70% of the changes in SST trends can be attributed to thermocline depth changes. The results confirm that the decadal changes of thermocline depth contribute to the interhemispheric gradient changes, especially to the increased warming in the southern Indian Ocean during the hiatus decade compared with the pre-hiatus decade.

b. Decadal changes in ITF transport and related variations in thermocline depth and SST

To further explore that relationship between the ITF, thermocline depth and SST in the southern Indian Ocean, we examine the time series of ITF transports from observations and four reanalysis products (Fig. 8). Negative ITF anomalies indicate more ITF transport from Pacific Ocean into Indian Ocean and positive anomalies less transport. All the four reanalysis products can reproduce the magnitudes and variations of the observed ITF transport during 2004-2006, with correlation coefficient statistically significant at the 95% level of confidence. The reanalyses show a decadally increasing ITF transport with the PDO transition from positive phase to negative phase in the late 1990s, consistent with previous studies (Lee et al. 2010, 2015).

The relationship between thermocline depth averaged over the southern Indian Ocean and ITF transport shows that they have the best correlation (-0.80) when ITF leads thermocline depth by about 48-months (Fig. 9). This lag relationship is qualitatively consistent with expectations from a simple two-dimensional mass balance for the Southern Hemisphere, integrated from the Indonesian passages to the African coast, i.e. $A\frac{\partial h}{\partial t}=-U$, where h is thermocline depth and U is ITF transport and A is the area affected by the ITF. This relationship indicates that decadal changes in thermocline depth adjust to anomalous ITF volume transports into the southern Indian Ocean at some lag.

To address the question of how the ITF transport contributes to thermocline changes in the Indian Ocean, we show the 48-month lagged regression pattern of thermocline depth anomaly onto decadally varying ITF transport (Fig. 10). Since the mean value of ITF transport is negative (i.e., into the Indian Ocean), negative regression coefficients indicate that more ITF transport corresponds to a deepening thermocline and less transport to a shoaling thermocline. These results clearly demonstrate that increased ITF transport during the recent global warming hiatus is associated with a deepening thermocline and elevated SST, consistent with the modeling results of Hirst and Godfrey (1993) and Lee et al. (2002) that increased ITF transport leads to a depression of the thermocline and warming SST between 10°S and 40°S in the Indian Ocean.

To estimate the magnitude of the ITF changes that lead to the observed changes in thermocline depth and SST during the hiatus decade, we compare decadal changes in ITF transport between 1996-2009 and 1984-1995 so as to account for the lagged response in the temperature field (Fig. 11). All the four reanalysis products indicate more ITF transport from Pacific Ocean to Indian Ocean during the most recent decade, though for GECCO2 it is a relatively small increase (Fig. 11). The mean increase in ITF transport of these four products is 0.91±0.70 Sv from 1984-1995 to 1996-2009, similar in magnitude to the model results of Lee et al. (2015) and the observed decadal changes in ITF transport based on XBT observations between Indonesia and northern Australia (Liu et al. 2015). Given the areal average regression slope over the southern Indian Ocean between thermocline depth and ITF transport is -2.82 m Sv^{-1} based on the 8 product mean (Fig. 10) and considering that the mean decadal increase in ITF is 0.91 Sv after 1996 (Fig. 11), the changes in thermocline depth due to this transport is about 2.6 m. This ITF-induced change accounts for more than 90% of the observed decadal change of mean thermocline depth (about 2.7 m) in the southern Indian Ocean (cf. Figs. 10 and 6) and thus are presumably the major contributor to the decadal changes of interhemispheric gradient in the Indian Ocean SST since the early 2000s (Fig. 2).

Increases in ITF transports over the past 30 years have been driven by increases in the strength of the Pacific trade winds associated with a phase transition of the PDO from positive to negative in the late 1990s (Feng et al. 2010, 2011; Lee et al. 2015). Variations in the Pacific trade winds are also dynamically linked to those in the Indian Ocean surface winds though the Walker circulation that spans the two basins (Han et al. 2014). In the next section we examine these wind field variations to determine what role Indian Ocean winds associated with the PDO may have played in contributing to decadal time scale thermocline depth and SST changes in the Indian

Ocean.

c. The role of large-scale Pacific and Indian Ocean wind stress variations

To clarify the relationship of Pacific decadal variations to decadal variations in the Indian Ocean, we examine the pattern of Indo-Pacific wind stress regressed onto the observed PDO index (Fig. 12). In the late 1990s, the PDO shifted phase from a positive to a negative (Fig. 12a). Corresponding to the negative PDO after 2000, anomalous easterly winds prevailed over the tropical Pacific, associated with an enhanced Walker circulation (Fig. 12b-e). The enhanced trade winds and Walker circulation associated with a negative phase PDO as well as the corresponding La Niña-like oceanic state have been discussed in previous studies (e.g. Luo et al. 2012; Sohn et al. 2013; England et al. 2014). Stronger trade winds piled up water in the western Pacific, elevating sea level there, creating the potential for enhanced ITF transport into the southern Indian Ocean via the Indonesian passages (Feng et al. 2011; England et al. 2014). The positive correlation of 0.86 (statistically significant at the 95% level of confidence) between decadal variations in the ITF and the PDO (Fig. 9) is consistent with this dynamical link (Lee et al. 2010).

Decadal changes in Indian Ocean winds between the hiatus decade (2000-2013) and pre-hiatus decade (1984-1999) (Figs. 13e-h) are very similar in pattern to Indian Ocean wind variations related to the PDO (Fig. 12), suggesting that the enhanced Walker circulation associated with the negative phase PDO during the recent hiatus decade is a main contributor to decadal changes in Indian Ocean winds through an atmospheric bridge between the two basins. Characteristics of these changes in Indian Ocean winds between the pre-hiatus and hiatus periods that are common to most of the wind products and their average include enhanced southeasterly winds at and south of 10°S, anomalous westerly winds along the equator, and enhanced southwesterly winds off east Africa north of the equator. Note that annual mean surface wind stresses north of 10°S in the Indian

Ocean are strongly affected by the seasonally intense winds associated with the Asian summer monsoon, so annual mean changes reflect those evident in the summer season (Figs. 13a-d). Thus, our results are consistent with those of Ueda et al. (2015), who described intensified southwesterly wind anomalies off east Africa north of the equator during the negative phase PDO in the summer season.

Comparing the climatology (Figs. 13a-d) with the decadal changes in Indian Ocean wind stress (Figs. 13e-h) indicates that the western flank of the Asian summer monsoon wind field is strengthened, while the central-eastern flanks towards the South Asian subcontinent are weakened. In addition, the pre-hiatus period in the Pacific was characterized by more El Niño-like conditions, while the recent hiatus period by La Nina-like conditions. El Niño conditions result in weak winds and warm SST anomalies in the tropical western Indian Ocean while La Niña conditions may not have an equally opposite impact, leading to some asymmetry in the Indian Ocean response to forcing through the Walker circulation during this period (Roxy et al. 2014). Nonetheless, observed decadal changes in wind stress lead to downwelling favorable (positive) wind stress curls in the Indian Ocean between 10^{o}S and 20^{o}S, west of 90^{o}E after 2000. These downwelling favorable winds would add to the thermocline deepening and SST warming related to the increase in ITF transport in that region (Figs. 13e-h). For the southern Indian Ocean as a whole though, the influence of downwelling wind stress curl is of secondary importance compared to the ITF in deepening the thermocline because it is confined to a much smaller region and is partially balanced by other areas of weak upwelling.

As discussed in Han et al. (2010), north of 10°S in the Seychelles Chagos Thermocline Ridge region, upwelling favorable wind stress curl would cause the thermocline to shoal, tending to cool SST there. Also, stronger winds off the coast of Somalia related to negative phase PDO conditions during the global warming hiatus would account for the shoaling thermocline along the Somalia coast (Fig. 6) and explain the coincidental anti-correlation between the PDO-related increased ITF transports and shallower thermocline depth (Fig. 10). The shallower thermocline though is associated with stronger density stratification and reduced vertical mixing in the thermocline of the western Arabian Sea (Roxy et al. 2016). Thus, while anomalous southwesterlies would intensify coastal upwelling and off-shore advection of upwelled water, the upwelled water may be coming from shallower depths and be warmer than it would otherwise be. During the hiatus decade therefore, the temperatures in this region are not actually cooling because of increased upwelling, but instead are warming less than in the pre-hiatus decade. Collectively, these regional Indian Ocean wind stress changes would contribute to a reduced warming trend in the northern Indian Ocean and an increased warming trend in the southern Indian Ocean, particularly between 10°S and 20°S, in the twenty-first century relative to the late twentieth century.

d. The role of surface heat fluxes and ITF-induced lateral heat advection

We next examine the role that surface heat fluxes might play in determining the interhemispheric gradient changes using four available surface heat flux products (Fig. 14). The decadal changes in surface net heat flux have a cooling effect in the northern Indian Ocean, consistent across all the four products. This cooling extends in all the products to about 20°S, south of which there is a tendency for the ocean to gain heat from the atmosphere in some regions.

The mean of the four products suggests that decadal changes in net surface heat flux favor the observed interhemispheric gradient in the Indian Ocean SST trend but with a boundary closer to 20°S rather than 10°S. We furthermore note that changes in net surface heat flux are mainly due to latent heat flux, which closely matches the pattern in net heat flux (Fig. 14). The factors that contribute to these changes in latent heat flux (i.e., surface wind speeds, stability effect, relative humidity, etc.) vary in importance among the products for reasons we do not fully understand. However, the reduced solar radiation expected from increasing anthropogenic aerosols as reported by Chung and Ramanathan (2006) are not obvious in our results (figure not shown). That may be because we are focusing on decadal time scales while they focused on the linear trend since the 1950s.

Based on the four products, the magnitude of the surface net heat flux change for the southern and northern Indian Ocean shows decrease of -1.48±0.33 W m^{-2} and -6.0±3.19 W m^{-2}, respectively, from the pre-hiatus to the hiatus decade (Fig. 14). The formal uncertainties in these estimates assume that the heat flux errors are random among the various products, but in fact the true errors may be much larger. Surface heat fluxes from reanalysis datasets may contain sizeable systematic errors, and the data coverage on which they are based is sparse, especially in the southern Indian Ocean (Harrison and Carson 2007). Also, assuming the decadal differences in SST trends are due solely to changes in surface heat fluxes, a 0.11±0.03 ^{o}C $decade^{-1}$ change in the southern Indian Ocean as observed would require an increase of 0.07±0.02 Wm^{-2} in net surface heat flux from the pre-hiatus decade to the recent hiatus decade. Likewise, a trend difference of -0.19±0.04 ^{o}C $decade^{-1}$ in the northern Indian Ocean would require a decrease of -0.12±0.03 Wm^{-2} in net surface heat flux. These estimates, based on assuming a mixed-layer depth as 50m (Lee et al. 2004), sea-water density as $1.025*10^{3}$ kg m^{-3} and specific heat at constant pressure as $4*10^{3}$ J kg^{-1} $^{o}C^{-1}$, are below the level of detectability. Thus, the magnitude the surface fluxes and their presumed impacts on SST are highly uncertain. Nevertheless, from the sign of the change in surface heat fluxes that north of 10°S and south of 20°S, one could infer that these fluxes would tend to reinforce observed SST trends, whereas between 10°S and 20°S, they may would act to damp SST trends.

Considering that increases in ITF transport not only deepen the thermocline, but also bring more warm water from the Pacific into the southern Indian Ocean, we need to distinguish between these two processes and how they affect southern Indian Ocean SSTs. To estimate the ITF contribution to horizontal advection in the mixed layer, we assume that anomalous heat transported into the Indian Ocean in the upper 50 m is distributed uniformly in the southern Indian Ocean between 10°-40°S, 40°-120°E (an area of $2.5*10^7$ km^2). ITF heat advection is then calculated for each of the four products (SODA2.2.4, GECCO2, ORA-S4, ORA-S3) using the temperature difference between the ITF inflow (8°-25°S along 113°E) and the areal mean of the southern Indian Ocean mixed layer temperature, following Zhang and McPhaden (2010). From this method, we estimate an increase in horizontal heat advection between the pre-hiatus and hiatus decades to be equivalent to 0.18±0.27 °C decade^{-1}. However, the contribution of horizontal advection via the Indonesian passages shows a large spread among the four products. Thus, the horizontal advection due to increased ITF may be important, but can't determine this with confidence due to its large spread. In contrast, the ITF-related vertical processes associated with thermocline depth anomaly obtained from Fig.7 results in a positive contribution of 0.08±0.006 °C decade^{-1} in the southern Indian Ocean and accounts for more than 70% of the observed changes in SST trends, which is robust among different products. Therefore, the influence of the increased ITF on warming the southern Indian Ocean SST is mainly from deepening the thermocline by more mass transport from the Pacific Ocean into the southern Indian Ocean, while the contribution of lateral warm advection is potentially important, though highly uncertain. A more detailed heat budget analysis for decadal changes in the interhemispheric SST gradient of Indian Ocean is beyond the scope of the present study, but will be carried out in a sequel to this work.

4. Summary and discussion

The main motivation of the present study is to clarify the characteristics of decadal changes in the interhemispheric gradient of SST trends in the Indian Ocean during the recent global warming hiatus compared with the pre-hiatus decade, and to highlight the mechanisms responsible for these changes. We have analyzed a wide variety of oceanic and atmospheric data sets to explore the potential role of forcing from the Pacific Ocean via the ITF and the atmospheric bridge involving the Walker circulation. Our main conclusions are that:

1) During the recent global warming hiatus, an interhemispheric gradient in SST trends appeared in the Indian Ocean, with relatively weak or little warming trend in the northern Indian Ocean and an enhanced warming trend in the southern Indian Ocean south of 10°S.

2) The interhemispheric gradient in the SST trend was mainly forced by an increase of ITF transport from the Pacific to the Indian Ocean. This increased transport led to a depression of the thermocline south of 10ºS that facilitated SST warming presumably through a reduced ability of vertical mixing to cool the surface in the southern Indian Ocean. This ITF-related deepened thermocline accounts for more than 70% of the observed increased warming trends in the southern Indian Ocean SST during the recent global warming hiatus compared with the pre-hiatus decade.

3) The wind stress and wind stress curl changes associated with an altered Walker circulation also played an important role. Along with the enhanced Walker circulation, anomalous easterly winds occurred at and south of 10°S, while anomalous westerly winds occurred along the equator. The resultant positive wind stress curl between 10ºS and 20ºS induced anomalous Ekman downwelling and the negative wind stress curl between 0° and 10ºS induced anomalous upwelling in the thermocline ridge region. In addition, anomalous southwesterly wind stress along the coast of Somalia would have intensified coastal upwelling and off shore advection of upwelled water in the northern Indian Ocean. This wind forcing would have favored warmer SSTs between 10ºS and

20°S and cooler SSTs to the north of 10°S, contributing to the interhemispheric gradient in SST trend. However, for the southern Indian Ocean as a whole though, the influence of wind stress curl is of secondary importance compared to the ITF because it is confined to a much smaller region and is partially balanced by other areas of weak upwelling.

4) Though highly uncertain, more loss of latent heat from the ocean to the atmosphere in the first decade of the twenty-first century would have contributed to a slowdown in SST warming north of 10°S. More advection of warm ITF surface water from the Pacific to the Indian Ocean, likewise highly uncertain, may also have played a role in the increased SST warming south of 10°S.

Many authors (Wang et al. 2012; Kosaka and Xie 2013; Meehl et al. 2013; Watanabe et al. 2014) have argued that the recent PDO cold phase in the Pacific, as well as the warming hiatus, were due to natural internal variability of the climate system. We have also attributed much of the decadal changes in ITF transport and surface wind stress in the Indian Ocean to changes in the Walker circulation related to PDO phase transitions. We thus infer that the resultant interhemispheric SST gradient change in the Indian Ocean is likewise primarily a reflection of natural internal decadal variability linked to the PDO. However, other changes coincident with but not necessarily related to PDO phase transitions may also be important and some of these may be anthropogenically forced. For example, the role of anthropogenic aerosols from South Asia in cooling the northern Indian Ocean (Barnett et al. 2005; Chung and Ramanathan 2006; Pierce et al. 2006) in competition with the effects of the anthropogenic radiative forcing due to GHG, may also affect the interhemispheric SST gradient (Chung and Ramanathan 2006). However, these effects are expected to operate on longer multi-decadal time scales than considered here. In addition, Goes et al. (2005) suggested that the enhanced southwesterly monsoonal winds off the coast of Somalia are the effect of an enhanced land-sea thermal gradient, which is governed by the reduced winter and spring snow cover over the Eurasian landmass forced by a mid-latitude continental warming trend reported in the Northern Hemisphere. The relative quantitative contributions of different factors, including both natural decadal variability and human-induced changes, in this key region of the world ocean therefore need further clarification.

We recognize that the Indian Ocean and Pacific Ocean are a coupled system in which the two can affect each other. This study mainly addressed the forcing effect of Pacific Ocean to Indian Ocean. However, the Indian Ocean plays an active role in affecting the Indo-Pacific climate during recent decades as well (Han et al. 2014). For example, the stronger warming in the tropical Indian Ocean than the Pacific Ocean favors enhanced trade winds over the Pacific (Luo et al. 2012), which may be related to the recent cooling in the eastern Pacific (England et al. 2014). Terray et al. (2015) indicates that warm SST anomalies in the Indian Ocean can dampen the magnitude and lifecycle of an El Niño event. This feedback from the Indian Ocean to the Pacific, which is beyond the scope of the present study, deserves further attention.

Acknowledgments

We thank three anonymous reviewers for very helpful comments on an earlier version of this manuscript. This research was performed while the first author held a National Research Council Research Associateship Award at NOAA/PMEL. This is PMEL contribution no. 4431.

References:

Alexander, M. A., I. Bladé, M. Newman, J. R. Lanzante, N. C. Lau, and J. D. Scott, 2002: The atmospheric bridge: The influence of ENSO teleconnections on air-sea interaction over the global oceans. *J. Climate,* **15(16),** 2205-2231, doi: 10.1175/1520-

0442(2002)015<2205:TABTIO>2.0.CO;2.

Alory, G., S. Wijffels, and G. Meyers, 2007: Observed temperature trends in the Indian Ocean over 1960–1999 and associated mechanisms. *Geophys. Res. Lett.,* **34,** L02606, doi:10.1029/2006GL028044.

Balmaseda, M. A., A. Vidard, and D. L. T. Anderson, 2008: The ECMWF Ocean Analysis System: ORA-S3. *Mon. Weather Rev.,* **136,** 3018-3034, doi:10.1175/2008MWR2433.1.

——, K. Mogensen, and A. T. Weaver, 2013: Evaluation of the ECMWF ocean reanalysis system ORAS4. *Q. J. R. Meteorol. Soc.,* **139(674),** 1132–1161, doi:10.1002/qj.2063.

Barnett, T. P., D. W. Pierce, K. M. Achutarao, P. J. Gleckler, B. D. Santer, J. M. Gregory, and W. M. Washington, 2005: Penetration of human-induced warming into the world's oceans. *Science,* **309,** 284–287, doi:10.1126/science.1112418.

Boyer, T. P., and Coauthors, 2009: World Ocean Database 2009, vol. 1, Introduction. *NOAA Atlas NESDIS,* vol. **66**, edited by S. Levitus, 219 pp., NOAA, Silver Spring, Md.

Cai, W., A. Sullivan, and T. Cowan, 2008: Shoaling of the off-equatorial south Indian Ocean thermocline: Is it driven by anthropogenic forcing? *Geophys. Res. Lett.,* **35(12),** L12711, doi:10.1029/2008GL034174.

Carton, J. A., and B. S. Giese, 2008: A reanalysis of ocean climate using simple ocean data assimilation (SODA). *Mon. Weather. Rev.,* **136(8),** 2999–3017, doi:10.1175/2007MWR1978.1.

Chung, C. E., and V. Ramanathan, 2006: Weakening of north Indian SST gradients and the monsoon rainfall in India and the Sahel. *J. Climate,* **19,** 2036–2045, doi:10.1175/JCLI3820.1.

Dee, D. P., and Coauthors, 2011: The ERA-Interim reanalysis: Configuration and performance of the data assimilation system. *Q. J. R. Meteorol. Soc.,* **137,** 553–597.

D'Mello, J. R., and S. P. Kumar, 2015: Why is the Bay of Bengal experiencing a reduced rate of sea surface warming? *International Journal of Climatology,* doi:10.1002/joc.4414.

Dong, L., and T. J. Zhou, 2014: The Indian Ocean Sea Surface Temperature Warming Simulated by CMIP5 Models during the 20th Century: Competing Forcing Roles of GHGs and Anthropogenic Aerosols. *J. Climate,* **27,** 3348–3362, doi:10.1175/JCLI-D-13-00396.1.

——, T. J. Zhou, and B. Wu, 2014: Indian Ocean warming during 1958-2004 simulated by a climate system model and its mechanism. *Clim. Dyn.,* **42,** 203-217, doi:10.1007/s00382-013-1722-z.

——, T. J. Zhou, A. G. Dai, F. F. Song, B. Wu, and X. L. Chen, 2016: The Footprint of the Inter-decadal Pacific Oscillation in Indian Ocean Sea Surface Temperatures. *Scientific Reports,* in press.

Du, Y., and S. P. Xie, 2008: Role of atmospheric adjustments in the tropical Indian Ocean warming during the 20th century in climate models. *Geophys. Res. Lett.,* **35,** L08712, doi:10.1029/2008GL033631.

Easterling, D. R., and M. F. Wehner, 2009: Is the climate warming or cooling? *Geophys. Res. Lett.,* **36,** L08706, doi:10.1029/2009GL037810.

England, M. H., S. McGregor, P. Spence, G. A. Meehl, A. Timmermann, W. Cai, A. Sen Gupta, M. J. McPhaden, A. Purich, and A. Santoso, 2014: Recent intensification of wind-driven circulation in the Pacific and the ongoing warming hiatus. *Nature Climate Change,* **4,** 222-227, doi:10.1038/nclimate2106.

Feng, M., M. J. McPhaden, and T. Lee, 2010: Decadal variability of the Pacific subtropical cells and their influence on the southeast Indian Ocean. *Geophys. Res. Lett.,* **37,** L09606, doi:10.1029/2010GL042796.

——, C. Böning, A. Biastoch, E. Behrens, E. Weller, and Y. Masumoto, 2011: The reversal of the multidecadal trends of the equatorial Pacific easterly winds, and the Indonesian Throughflow and Leeuwin Current transports. *Geophys. Res. Lett.,* **38,** L11604, doi:10.1029/2011GL047291.

Giese, B. S., and S. Ray, 2011: El Niño variability in simple ocean data assimilation (SODA), 1871–2008. *J. Geophys. Res.-Oceans, (1978–2012),* **116(C2),** doi: 10.1029/2010JC006695.

Goes, J. I., P. G. Thoppil, do R. Gomes, and J. T. Fasullo, 2005: Warming of the Eurasian landmass is making the Arabian Sea more productive. *Science,* **308(5721),** 545–547, doi:10.1126/science.1106610.

Good, S. A., M. J. Martin, and N. A. Rayner, 2013: EN4: Quality controlled ocean temperature and salinity profiles and monthly objective analyses with uncertainty estimates. *J. Geophys. Res.-Oceans,* **118,** 6704–6716, doi: 10.1002/2013jc009067.

Han, W. Q., and Coauthors, 2010: Patterns of Indian Ocean sea-level change in a warming climate. *Nature Geoscience,* **3(8),** 546-550, doi:10.1038/ngeo901.

——, J. Vialard, M. J. McPhaden, T. Lee, Y. Masumoto, M. Feng, and W. P. M. de Ruijter, 2014: Indian Ocean Decadal Variability: A Review. *Bull. Amer. Meteor. Soc.,* **95,** 1679-1703, doi: 10.1175/BAMS-D-13-00028.1.

Harrison, D. E., and M. Carson, 2007: Is the world ocean warming? Upper ocean trends, 1950–2000. *J. Phys. Oceanogr.,* **37,** 174–187, doi:10.1175/JPO3005.1.

Hirst, A. C., and J. S. Godfrey, 1993: The role of Indonesian throughflow in a global ocean GCM. *Journal of Physical Oceanography,* **23(6),** 1057-1086, doi: 10.1175/1520-0485(1993)023<1057:TROITI>2.0.CO;2.

Hoerling, M., J. W. Hurrell, T. Xu, G. T. Bates, and A. S. Phillips, 2004: Twentieth century North Atlantic climate change. Part II: Understanding the effect of Indian Ocean warming. *Clim. Dyn.* **23**, 391–405, doi:10.1007/s00382-004-0433-x.

Ishii, M., A. Shouji, S. Sugimoto, T. Matsumoto, 2005: Objective analyses of sea-surface temperature and marine meteorological variables for the 20th century using ICOADS and the Kobe Collection. *Int. J. Climatol.,* **25,** 865–879, doi:10.1002/joc.1169.

Kanamitsu, M., W. Ebisuzaki, J. Woollen, S.-K. Yang, J. J. Hnilo, M. Fiorino, and G. L. Potter, 2002: NCEP–DOE AMIP-II reanalysis (R-2). *Bull. Amer. Meteor. Soc.,* **83,** 1631–1643, doi:10.1175/BAMS-83-11-1631.

Kaplan, A., M. A. Cane, Y. Kushnir, A. C. Clement, M. B. Blumenthal, and B. Rajagopalan, 1998: Analyses of global sea surface temperature 1856–1991. *J. Geophys. Res.,* **103,** 18567–18589, doi:10.1029/97JC01736.

Kennedy, J. J., N. A. Rayner, R. O. Smith, D. E. Parker, and M. Saunby, 2011a: Reassessing biases and other uncertainties in sea surface temperature observations measured in situ since 1850: 1. Measurement and sampling uncertainties. *J. Geophys. Res.,* **116,** D14103, doi:10.1029/2010JD015218.

——, N. A. Rayner, R. O. Smith, D. E. Parker, and M. Saunby, 2011b: Reassessing biases and other uncertainties in sea surface temperature observations measured in situ since 1850: 2. Biases and homogenization. *J. Geophys. Res.,* **116,** D14104, doi:10.1029/2010JD015220.

Köhl, A., 2015: Evaluation of the GECCO2 ocean synthesis: transports of volume, heat and freshwater in the Atlantic. *Q. J. R. Meteorol. Soc.,* **141,** 166–181, doi:10.1002/qj.2347.

Kosaka, Y., and S. P. Xie, 2013: Recent global-warming hiatus tied to equatorial Pacific surface cooling. *Nature,* **501**, 403–407, doi: 10.1038/nature12534.

Krishnan, R., K. V. Ramesh, B. K. Samala, G. Meyer, J. M. Slingo, and M. J. Fennessy, 2006: Indian Ocean–monsoon coupled interactions and impending monsoon droughts. *Geophys. Res. Lett.,* **33**, L08711, doi:10.1029/2006GL025811.

Kumar, B. P., and Coauthors, 2012: TropFlux: air-sea fluxes for the global tropical oceans—description and evaluation. *Climate Dynamics,* **38(7),** 1521-1543, doi:10.1007/s00382-011-1115-0.

Lee, S. K., W. Park, M. O. Baringer, A. L. Gordon, B. Huber, and Y. Liu, 2015: Pacific origin of the abrupt increase in Indian Ocean heat content during the warming hiatus. *Nature Geoscience,* **8,** 445-449, doi:10.1038/ngeo2438.

Lee, T., I. Fukumori, D. Menemenlis, Z. Xing, and L. L. Fu, 2002: Effects of the Indonesian throughflow on the Pacific and Indian Oceans. *Journal of Physical Oceanography,* **32(5),** 1404-1429, doi:10.1175/1520-0485(2002)032<1404:EOTITO>2.0.CO;2

——, I. Fukumori, and B. Tang, 2004: Temperature advection: Internal versus external processes. *Journal of physical oceanography,* **34(8),** 1936-1944, doi: 10.1175/1520-0485(2004)034<1936:TAIVEP>2.0.CO;2

——, and M. J. McPhaden, 2008: Decadal phase change in large-scale sea level and winds in the Indo-Pacific region at the end of the 20th century. *Geophys. Res. Lett.,* **35,** L01605, doi:10.1029/2007GL032419.

——, and Coauthors, 2010: Consistency and fidelity of Indonesian-throughflow total volume transport estimated by 14 ocean data assimilation products. *Dynamics of Atmospheres and Oceans,* **50(2),** 201-223, doi:10.1016/j.dynatmoce.2009.12.004.

Levitus, S., and Coauthor, 2012: World ocean heat content and thermosteric sea level change (0–2000 m), 1955–2010. *Geophys. Res. Lett.,* **39,** L10603, doi:10.1029/2012GL051106.

Li, Y. L., and W. Q. Han, 2015: Decadal Sea Level Variations in the Indian Ocean Investigated with HYCOM: Roles of Climate Modes, Ocean Internal Variability, and Stochastic Wind Forcing. *J. Climate,* **28(23),** 9143-9165, doi:10.1175/JCLI-D-15-0252.1.

Liu, Q. Y., M. Feng, D. Wang, and S. Wijffels, 2015: Interannual variability of the Indonesian Throughflow transport: A revisit based on 30 year expendable bathythermograph data. *J. Geophys. Res. Oceans,* **120,** 8270–8282, doi:10.1002/2015JC011351.

Luo, J. J., W. Sasakia, and Y. Masumoto, 2012: Indian Ocean warming modulates Pacific climate change. *PNAS,* **109,** 18701–18706, doi:10.1073/pnas.1210239109.

Lyon, B., and D. G. DeWitt, 2012: A recent and abrupt decline in the East African long rains. *Geophys. Res. Lett.,* **39**, L02702, doi:10.1029/2011GL050337.

Meehl, G. A., J. M. Arblaster, J. T. Fasullo, A. Hu, and K. E. Trenberth, 2011: Model-based evidence of deep-ocean heat uptake during surface-temperature hiatus periods. *Nature Climate Change,* **1(7),** 360-364, doi:10.1038/nclimate1229.

——, A. Hu, J. M. Arblaster, J. Fasullo, and K. E. Trenberth, 2013: Externally forced and internally generated decadal climate variability associated with the Interdecadal Pacific Oscillation. *J. Climate,* **26,** 7298-7310, doi:10.1175/JCLI-D-12-00548.1.

Nidheesh, A. G., M. Lengaigne, J. Vialard, A. S. Unnikrishnan, and H. Dayan, 2013: Decadal and long-term sea level variability in the tropical Indo-Pacific Ocean. *Clim. Dyn.,* **41,** 381-402, doi:10.1007/s00382-012-1463-4.

Nieves, V., J. K. Willis, and W. C. Patzert, 2015: Recent hiatus caused by decadal shift in Indo-Pacific heating. *Science,* **349(6247),** 532-535, doi:10.1126/science.aaa4521.

Nishida, T., T. Kitakado, and H. Matsuura, 2011: Validation of the Global Ocean Data Assimilation System (GODAS) data in the NOAA National Centre for Environmental System (NCEP) by theory, comparative studies, applications and sea truth. IOTC-2011-WPB09-11.

Pierce, D. W., T. P. Barnett, K. AchutaRao, P. Gelckler, J. Gregory, and W. Washington, 2006: Anthropogenic warming of the oceans: Observations and model results. *J. Climate,* **19,** 1873–1900, doi:10.1175/JCLI3723.1.

Rayner, N. A., D. E. Parker, E. B. Horton, C. K. Folland, L. V. Alexander, D. P. Rowell, E. C. Kent, and A. Kaplan, 2003: Global analyses of sea surface temperature, sea ice, and night marine air temperature since the late nineteenth century. *J. Geophys. Res.,* **108(D14),** 4407, doi:10.1029/2002JD002670.

Reason, C. J. C., R. J. Allan, and J. A. Lindesay, 1996: Evidence for the influence of remote forcing on interdecadal variability in the southern Indian Ocean. *J. Geophys. Res.,* **101(C5),** 11867–11882, doi:10.1029/96JC00122.

Reynolds, R. W., N. A. Rayner, T. M. Smith, D. C. Stokes, and W. Wang, 2002: An improved in situ and satellite SST analysis for climate. *J. Climate,* **15,** 1609-1625, doi:10.1175/1520-0442(2002)015<1609:AIISAS>2.0.CO;2.

Roxy, M. K., K. Ritika, P. Terray, S. Masson, 2014: The curious case of Indian Ocean warming. *J. Climate,* **27,** 8501-8509, doi: 10.1175/JCLI-D-14-00471.1.

——, K. Ritika, P. Terray, R. Murutugudde, K. Ashok, and B. N. Goswami, 2015: Drying of Indian subcontinent by rapid Indian Ocean warming and a weakening land-sea thermal gradient. *Nature Communications,* **6,** 7423, doi:10.1038/ncomms8423.

——, A. Modi, R. Murtugudde, V. Valsala, S. Panickal, S. Prasanna Kumar, M. Ravichandran, M. Vichi, and M. Lévy, 2016: A reduction in marine primary productivity driven by rapid warming over the tropical Indian Ocean. *Geophys. Res. Lett.,* **43,** doi:10.1002/2015GL066979.

Schott, F. A., S. P. Xie, and J. P. McCreary, 2009: Indian Ocean circulation and climate variability. *Reviews of Geophysics,* **47(1),** doi:10.1029/2007RG000245.

Schwarzkopf, F. U., and C. W. Böning, 2011: Contribution of Pacific wind stress to multi‐decadal variations in upper-ocean heat content and sea level in the tropical south Indian Ocean. *Geophys. Res. Lett.,* **38,** L12602, doi:10.1029/2011GL047651.

Smith, T. M., R. W. Reynolds, T. C. Peterson, and J. Lawrimore, 2008: Improvements to NOAA's historical merged land-ocean surface temperature analysis (1880–2006). *J. Clim.,* **21,** 2283–2296, doi:10.1175/2007JCLI2100.1.

Sohn, B. J., S. W. Yeh, J. Schmetz, and H. J. Song, 2013: Observational evidences of Walker circulation change over the last 30 years contrasting with GCM results. *Climate Dynamics,* **40(7-8),** 1721-1732, doi:10.1007/s00382-012-1484-z.

Sprintall, J., S. E. Wijffels, R. Molcard, I. Jaya, 2009: Direct estimates of the Indonesian throughflow entering the Indian Ocean: 2004–2006. *J. Geophys. Res.,* **114,** C7, doi:10.1029/2008JC005257.

Terray, P., S. Masson, C. Prodhomme, M. K. Roxy, K. P. Sooraj, 2015: Impacts of Indian and Atlantic oceans on ENSO in a comprehensive modeling framework. *Climate Dynamics,* **46(7),** 2507-2533, doi:10.1007/s00382-015-2715-x.

Trenary, L., and W. Han, 2013: Local and remote forcing of decadal sea level and thermocline depth variability in the south Indian Ocean. *J. Geophys. Res.,* **118,** 381-398, doi:10.1029/2012JC008317.

Ueda, H., Y. Kamae, M. Hayasaki, A. Kitoh, S. Watanabe, Y. Miki, and A. Kumai, 2015: Combined effects of recent Pacific cooling and Indian Ocean warming on the Asian monsoon. *Nature communications,* **6,** doi:10.1038/ncomms9854.

Wang, B., J. Liu, H. J. Kim, P. J. Webster, and S. Y. Yim, 2012: Recent change of the global monsoon precipitation (1979–2008). *Clim. Dyn.,* **39,** 1123–1135, doi:10.1007/s00382-011-1266-z.

Watanabe, M., H. Shiogama, H. Tatebe, M. Hayashi, M. Ishii, and M. Kimoto, 2014: Contribution of natural decadal variability to global warming acceleration and hiatus. *Nature Climate Change,* **4,** 893–897, doi:10.1038/nclimate2355.

Wijffels, S., and G. Meyers, 2003: Fifteen years of XBT measurements in the Indonesian Throughflow. *CSIRO Marine Research.*

Yu, L., and M. M. Rienecker, 1999: Mechanisms for the Indian Ocean warming during the 1997–98 El Nino. *Geophys. Res. Lett.,* **26(6),** 735-738, doi:10.1029/1999GL900072.

——, X. Jin, and R. A. Weller, 2008: Multidecade Global Flux Datasets from the Objectively Analyzed Air-sea Fluxes (OAFlux) Project: latent and sensible heat fluxes, ocean evaporation, and related surface meteorological variables. OAFlux Project Technical Report OA-2008-01, Woods Hole Oceanographic Institution, Woods Hole, MA, 64 pp.

Zhang, X., and M. J. McPhaden, 2010: Surface layer heat balance in the Eastern Equatorial Pacific Ocean on Interannual Time Scales: influence of local versus remote wind forcing. *Journal of Climate*, **23(16),** 4375-4394, doi:10.1175/2010JCLI3469.1.

Zhou, T. J., R. Yu, J. Zhang, H. Drange, C. Cassou, C. Deser, D. L. R. Hodson, E. Sanchez-Gomez, J. Li, N. Keenlyside, X. Xin, and Y. Okumura, 2009: Why the Western Pacific Subtropical High has extended westward since the late 1970s. *J. Clim.,* **22**, 2199–2215, doi:10.1175/2008JCLI2527.1.

Figure Captions:

Fig. 1 Time series (a, b) in units of ^{o}C and linear trends (c, d) in units of ^{o}C decade^{-1} for annual mean SST anomalies averaged in the northern Indian Ocean (10^{o}S-30^{o}N, 40-120^{o}E) and southern Indian Ocean (10-40^{o}S, 40-120^{o}E) from HadISST (orange lines), Kaplan_V2 (blue lines), ERSST_v3b (red lines), HadSST3 (green lines), OISST_V2 (yellow lines), TropFlux (pink lines) and 6 products mean (thick black lines). The error bars in (c, d) denote the 95% confidence limits based on the 6 different data sets.

Fig. 2 Time series of 7-year running mean of PDO index and 15-year running trend (in ^{o}C decade^{-1}) in SST differences between the northern Indian Ocean (10^{o}S-30^{o}N, 40-120^{o}E) and southern Indian Ocean (10-40^{o}S, 40-120^{o}E) from 4 longer time products mean (HadISST, Kaplan_V2, ERSST_v3b, HadSST3). The shading is plus to minus one standard deviation based on the 4 datasets. The centered years for each trend are shown as x-axis.

Fig. 3 The SST trends (in ^{o}C decade^{-1}) during the pre-hiatus decade (1984-1999) from (a) HadISST, (b) Kaplan_V2, (c) ERSST_v3b, (d) HadSST3, (e) OISST_V2, (f) TropFlux and (g) 6 product mean. The dotted areas in (a-f) indicate the linear trends are statistically significant at the 95% level of confidence from a two sided Student t-test, those in (g) indicate the mean of the 6 products is greater than their standard error. The dashed lines denote the separation between the northern and southern Indian Ocean as defined for the purpose of this study.

Fig. 4 Same as Fig. 3, but for the trends during the recent hiatus decade (2000-2013).

Fig. 5 The differences of SST trends (in ^{o}C decade^{-1}) between the hiatus decade (2000-2013) and pre-hiatus decade (1984-1999) from (a) HadISST, (b) Kaplan_V2, (c) ERSST_v3b, (d) HadSST3, (e) OISST_V2, (f) TropFlux and (g) 6 product mean. The dotted areas in (g) indicate the mean of the 6 products is greater than their standard error. Black solid lines denote the climatological 28^{o}C isotherm, which is not provided in Kapnlan_v2 and HadSST3.

Fig. 6 The differences of mean thermocline depth between the hiatus decade (2000-2013) and pre-hiatus decade (1984-1999) from (a) WOD, (b) Ishii, (c) EN4, (d) GODAS, (e) ORA-S4, (f) SODA2.2.4, (g) ORA-S3, (h) GECCO2, (i) eight product mean. Stippling in (a-h) indicates the decadal changes are statistically significant at the 95% level of confidence from a two sided Student t-test. The dotted areas in (i) indicate the mean of the 8 products is greater than their standard error. Black solid lines in (i) denote the 1984-2014 mean of thermocline depth. Units: m

Fig. 7 Time series of 15-year running trend (a) SST and (b) thermocline depth averaged in the southern Indian Ocean (10-40ºS, 40-120ºE). (c) The changes of SST trends (in ºC $decade^{-1}$) induced by thermocline depth between the hiatus decade (2000-2013) and pre-hiatus decade (1984-1999). The changes are obtained by regressing 15-year SST running trend onto the 15-year running trend in thermocline depth, then multiplied the regression pattern with the decadal changes of thermocline depth trends between the hiatus decade (2000-2013) and pre-hiatus decade (1984-1999) at each grid point. Note that we use 4 SST datasets (HadISST, Kaplan_V2, ERSST_v3b and HadSST3) and 8 products of the thermocline depth (WOD, Ishii, EN4, GODAS, ORA-S4, SODA2.2.4, ORA-S3, GECCO2). Red lines in (a, b) represent the mean of all the products and figure (c) is the mean of 32 regression patterns from the 4 SST and 8 thermocline depth products. Stippling indicates the mean of the 32 regression patterns is greater than their standard error.

Fig. 8 Time series of total-depth vertically integrated volume transport by ITF based on the monthly data of (a) INSTANT, (b) SODA2.2.4, (c) GECCO2, (d) ORA-S4, and (e) ORA-S3. The red lines denote an 85-month running mean low pass filter (approximately 7-year) to eliminate year-to-year variations related to ENSO, with the scale shown on the right axes. The "mean" values given in the top-right denote the mean during 2004-2006 based on monthly data from each product and "corr" in (b-e) indicates the correlation coefficient with the INSTANT time series (with the correlations after linear trend removal shown in the parentheses) after removing the annual cycle. All correlations are statistically different from zero at the 95% level of confidence. Transport is in units of Sverdrup (1 Sv = 10^6 m^3 s^{-1}).

Fig. 9. Time series of 85-month running mean (approximately 7-year to eliminate year-to-year variations) total-depth vertically integrated volume transport by Indonesian Throughflow (ITF) based on the monthly data of four products mean (SODA2.2.4, GECCO2, ORA-S4, ORA-S3; red line), PDO index (blue line), and thermocline depth based on monthly data of seven products mean (Ishii, EN4, GODAS, ORA-S4, SODA2.2.4, ORA-S3, GECCO2) averaged in the southern Indian Ocean (10-40ºS, 40-120ºE; black line). The shading is plus-minus one standard deviation based on all the products used.

Fig. 10 The regression pattern of 48-month lag thermocline depth onto ITF transport smoothed with an 85-month running mean filter (approximately 7-year to eliminate year-to-year variations) during 1984-2014 from (a) WOD, (b) Ishii, (c) EN4, (d) GODAS, (e) ORA-S4, (f) SODA2.2.4, (g) ORA-S3, (h) GECCO2, (i) eight product mean. Note that the ITF transport used to regress against the data (a-d) is from ORA-S3 as it shows the largest correlation coefficient and closest mean value to INSTANT (Fig. 8), while transports used in (e-h) are based on each product, respectively. To compare with Fig. 6, the color is inverted. Stippling indicates differences that are significantly different from zero with 95% confidence based on a Student t-test. The areal average over the southern Indian Ocean (10-40ºS, 40-120ºE) regression slope for the 8 product mean is -2.82 m Sv^{-1}. Units: m Sv^{-1}

Fig. 11 The differences of mean ITF transport with 4 years earlier than the decades we used for the SST, as the differences between 1996-2009 and 1984-1995 from SODA2.2.4, GECCO2, ORA-S4 and ORA-S3. The dashed line indicates the mean of the four products. Units: Sv = 10^6 m^3 s^{-1}.

Fig. 12 (a) PDO index during 1984-2014 with monthly values shown as black line and 85-month running mean (approximately 7-year to eliminate year-to-year variations) shown as red line. The regression pattern of surface wind stress onto the 85-month running mean PDO index for (b) SODA2.2.4, (c) TropFlux, (d) ERA Interim and (e) the three product mean. Note that the regression patterns in (b-e) correspond to negative phase of PDO. Units in (b)-(e) are N m^{-2}

Fig. 13 (a-d) The climatology of surface wind stress (vector, units: N m^{-2}) and its curl (shading, units: 10^{-7} N m^{-3}), (e-h) differences of mean surface wind stress and its curl (units: 10^{-8} N m^{-3}) between the hiatus decade (2000-2013) and pre-hiatus decade (1984-1999) from (a, e) SODA2.2.4, (b, f) TropFlux, (c, g) ERA Interim, (d, h) 3 product mean. Stippling indicates differences that are significantly different from zero with 95% confidence based on a Student t-test.

Fig. 14 The differences of mean surface net heat flux (left) and latent heat flux (right) between the hiatus decade (2000-2013) and pre-hiatus decade (1984-1999) from (a, b) OAFlux, (c, d) TropFlux, (e, f) NCEP2, (g, h) ERA Interim, (i, j) four product mean. Setting downward (warming SST) is positive. Stippling indicates differences that are significantly different from zero with 95% confidence based on a Student t-test. Units: W m^{-2}

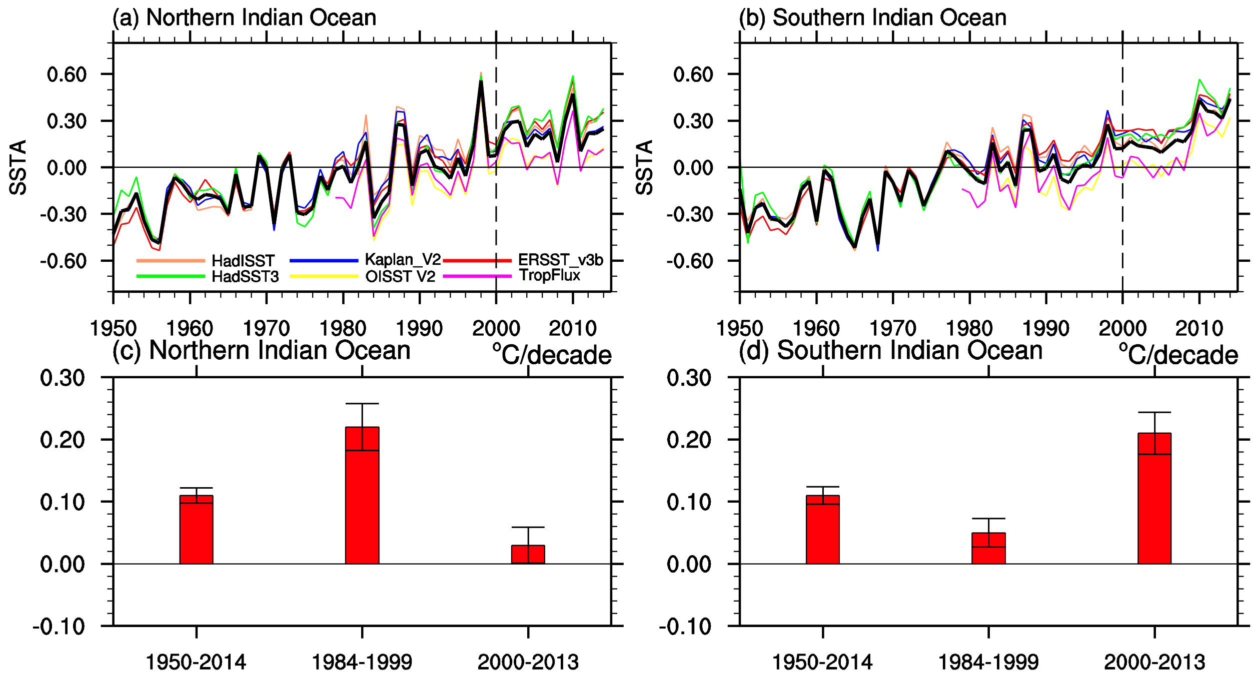

Fig. 1 Time series (a, b) in units of °C and linear trends (c, d) in units of °C decade^{-1} for annual mean SST anomalies averaged in the northern Indian Ocean (10°S-30°N, 40-120°E) and southern Indian Ocean (10-40°S, 40-120°E) from HadISST (orange lines), Kaplan_V2 (blue lines), ERSST_v3b (red lines), HadSST3 (green lines), OISST_V2 (yellow lines), TropFlux (pink lines) and 6 products mean (thick black lines). The error bars in (c, d) denote the 95% confidence limits based on the 6 different data sets.

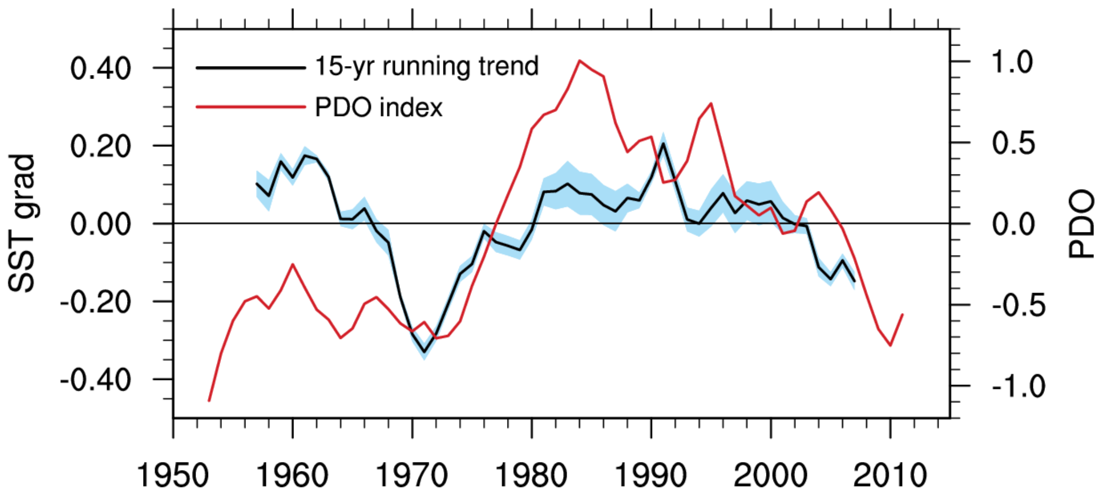

Fig. 2 Time series of 7-year running mean of PDO index and 15-year running trend (in ^{o}C decade^{-1}) in SST differences between the northern Indian Ocean (10^{o}S-30^{o}N, 40-120^{o}E) and southern Indian Ocean (10-40^{o}S, 40-120^{o}E) from 4 longer time products mean (HadISST, Kaplan_V2, ERSST_v3b, HadSST3). The shading is plus to minus one standard deviation based on the 4 datasets. The centered years for each trend are shown as x-axis.

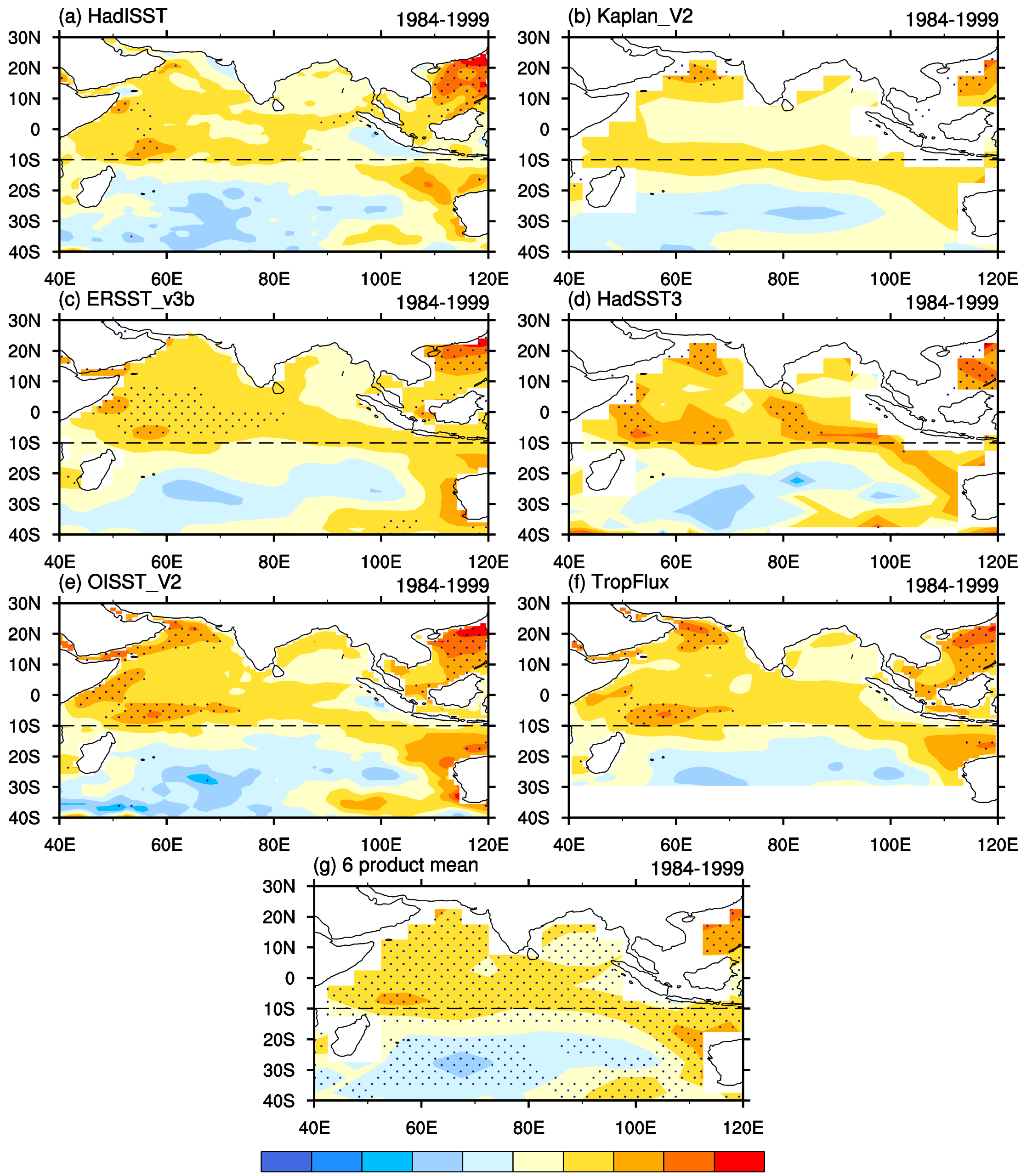

Fig. 3 The SST trends (in ^{o}C decade^{-1}) during the pre-hiatus decade (1984-1999) from (a) HadISST, (b) Kaplan_V2, (c) ERSST_v3b, (d) HadSST3, (e) OISST_V2, (f) TropFlux and (g) 6 product mean. The dotted areas in (a-f) indicate the linear trends are statistically significant at the 95% level of confidence from a two sided Student t-test, those in (g) indicate the mean of the 6 products is greater than their standard error. The dashed lines denote the separation between the northern and southern Indian Ocean as defined for the purpose of this study.

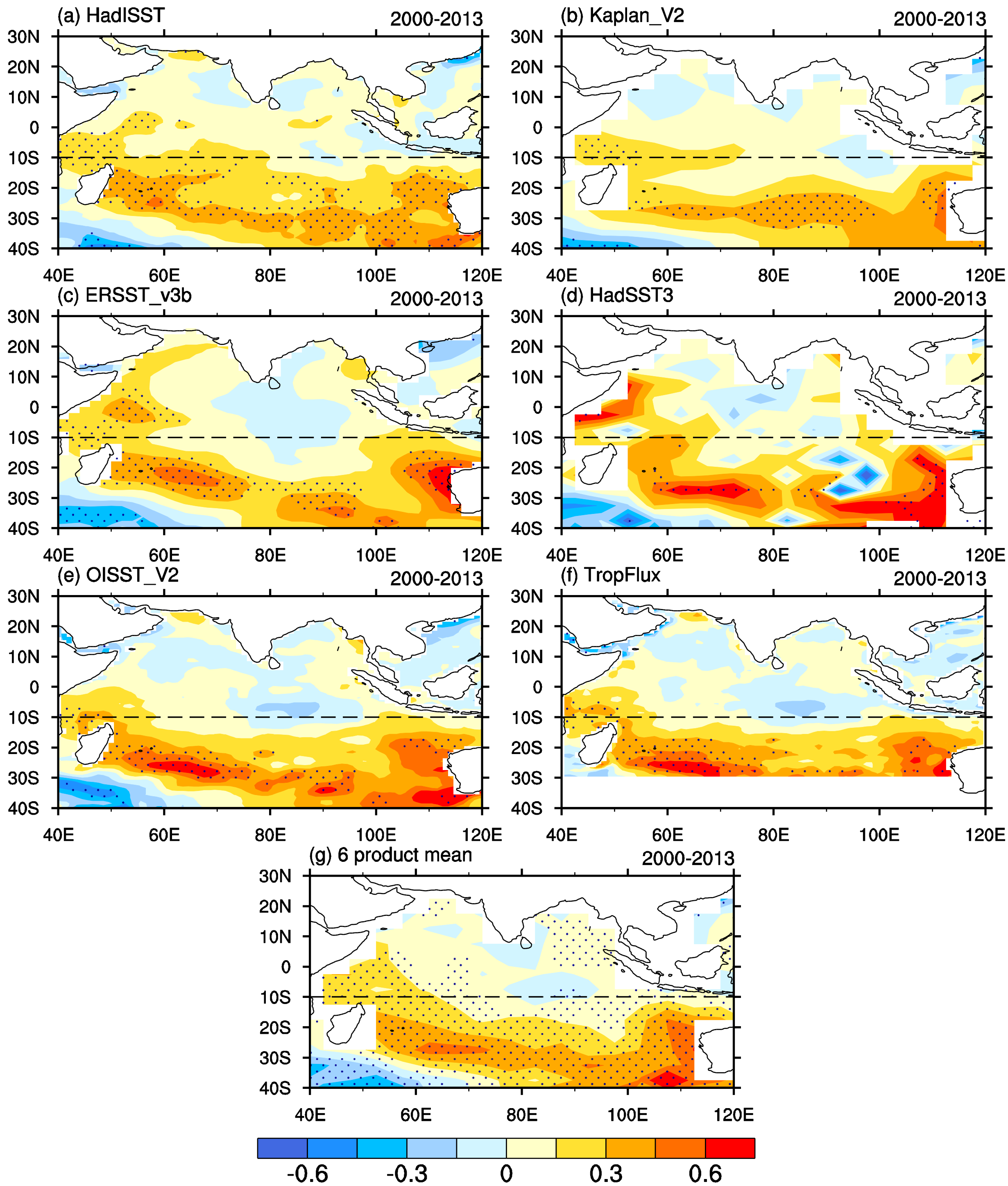

788

789

790 **Fig. 4** Same as Fig. 3, but for the trends during the recent hiatus decade (2000-2013).

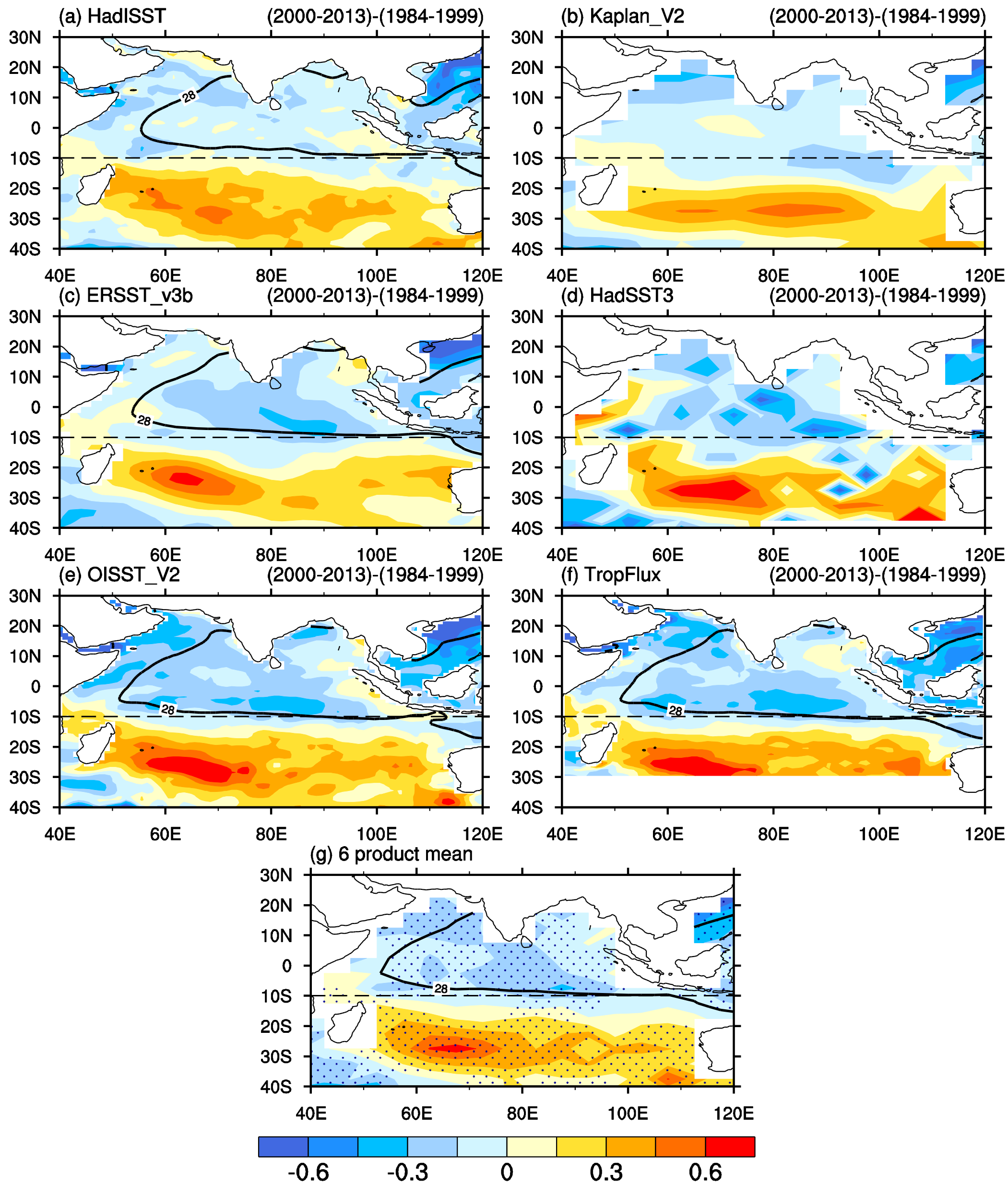

Fig. 5 The differences of SST trends (in ^{o}C $decade^{-1}$) between the hiatus decade (2000-2013) and pre-hiatus decade (1984-1999) from (a) HadISST, (b) Kaplan_V2, (c) ERSST_v3b, (d) HadSST3, (e) OISST_V2, (f) TropFlux and (g) 6 product mean. The dotted areas in (g) indicate the mean of the 6 products is greater than their standard error. Black solid lines denote the climatological $28^{o}C$ isotherm, which is not provided in Kapnlan_v2 and HadSST3.

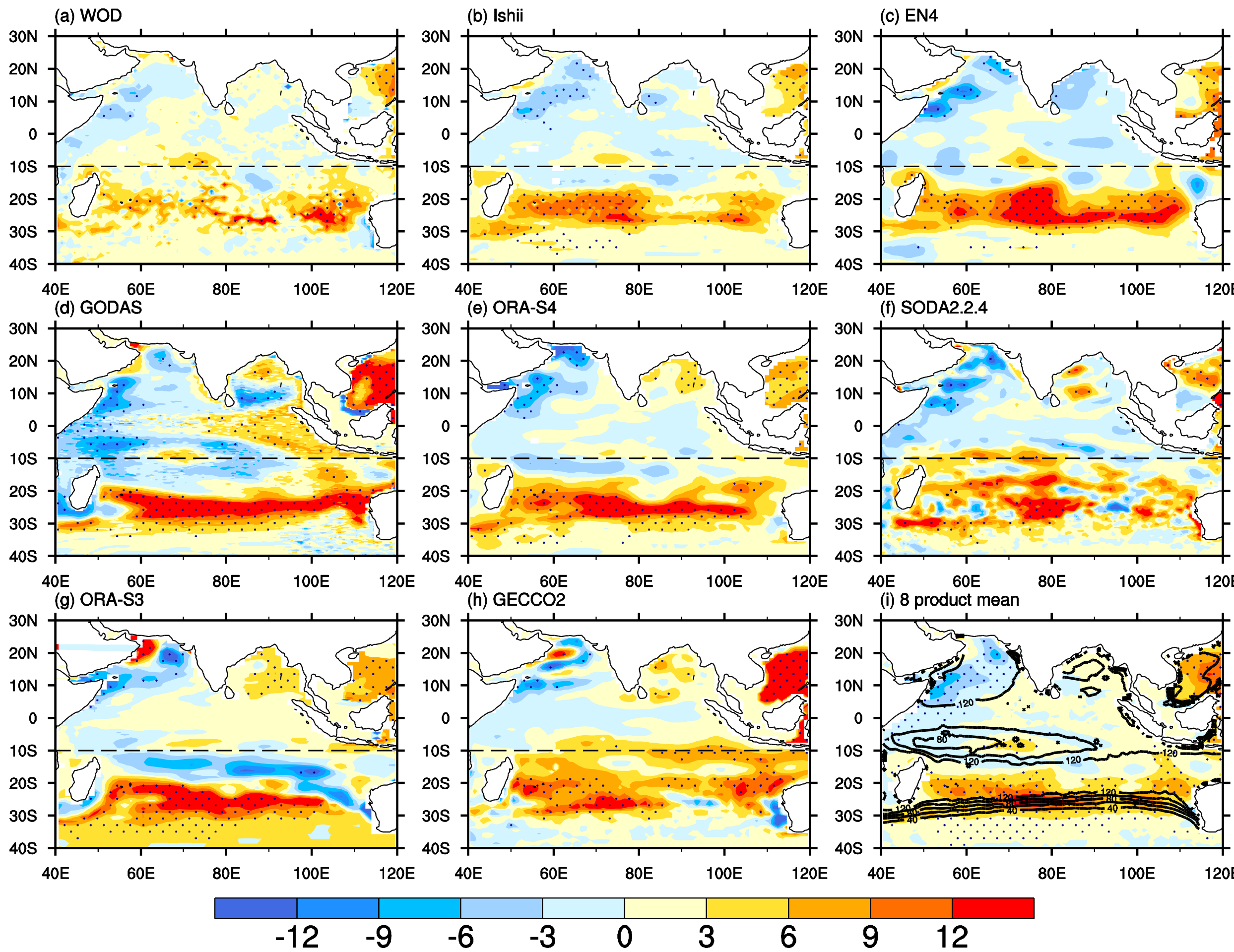

Fig. 6 The differences of mean thermocline depth between the hiatus decade (2000-2013) and pre-hiatus decade (1984-1999) from (a) WOD, (b) Ishii, (c) EN4, (d) GODAS, (e) ORA-S4, (f) SODA2.2.4, (g) ORA-S3, (h) GECCO2, (i) eight product mean. Stippling in (a-h) indicates the decadal changes are statistically significant at the 95% level of confidence from a two sided Student t-test. The dotted areas in (i) indicate the mean of the 8 products is greater than their standard error. Black solid lines in (i) denote the 1984-2014 mean of thermocline depth. Units: m

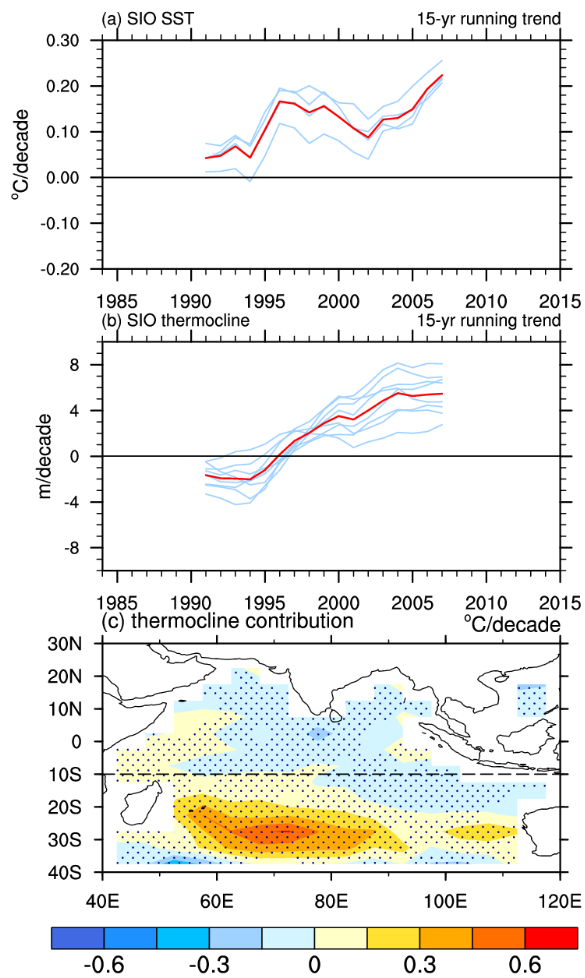

Fig. 7 Time series of 15-year running trend (a) SST and (b) thermocline depth averaged in the southern Indian Ocean (10-40°S, 40-120°E). (c) The changes of SST trends (in °C decade^{-1}) induced by thermocline depth between the hiatus decade (2000-2013) and pre-hiatus decade (1984-1999). The changes are obtained by regressing 15-year SST running trend onto the 15-year running trend in thermocline depth, then multiplied the regression pattern with the decadal changes of thermocline depth trends between the hiatus decade (2000-2013) and pre-hiatus decade (1984-1999) at each grid point. Note that we use 4 SST datasets (HadISST, Kaplan_V2, ERSST_v3b and HadSST3) and 8 products of the thermocline depth (WOD, Ishii, EN4, GODAS, ORA-S4, SODA2.2.4, ORA-S3, GECCO2). Red lines in (a, b) represent the mean of all the products and figure (c) is the mean of 32 regression patterns from the 4 SST and 8 thermocline depth products. Stippling indicates the mean of the 32 regression patterns is greater than their standard error.

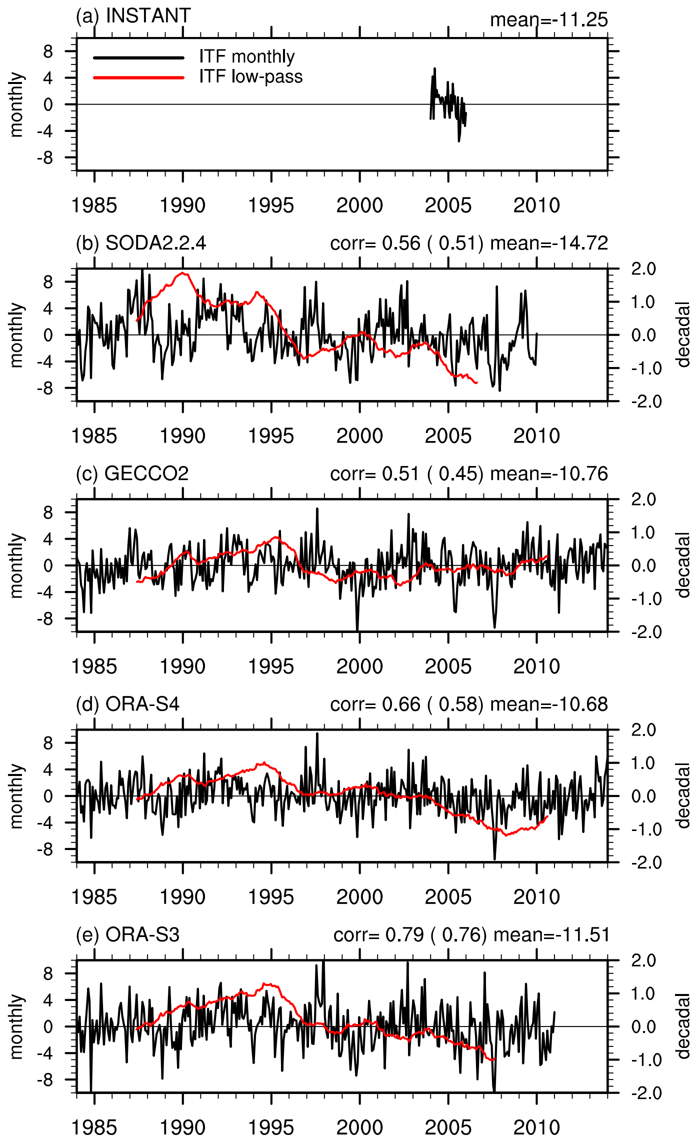

Fig. 8 Time series of total-depth vertically integrated volume transport by ITF based on the monthly data of (a) INSTANT, (b) SODA2.2.4, (c) GECCO2, (d) ORA-S4, and (e) ORA-S3. The red lines denote an 85-month running mean low pass filter (approximately 7-year) to eliminate year-to-year variations related to ENSO, with the scale shown on the right axes. The "mean" values given in the top-right denote the mean during 2004-2006 based on monthly data from each product and "corr" in (b-e) indicates the correlation coefficient with the INSTANT time series (with the correlations after linear trend removal shown in the parentheses) after removing the annual cycle. All correlations are statistically different from zero at the 95% level of confidence. Transport is in units of Sverdrup (1 Sv = 10^6 m^3 s^{-1}).

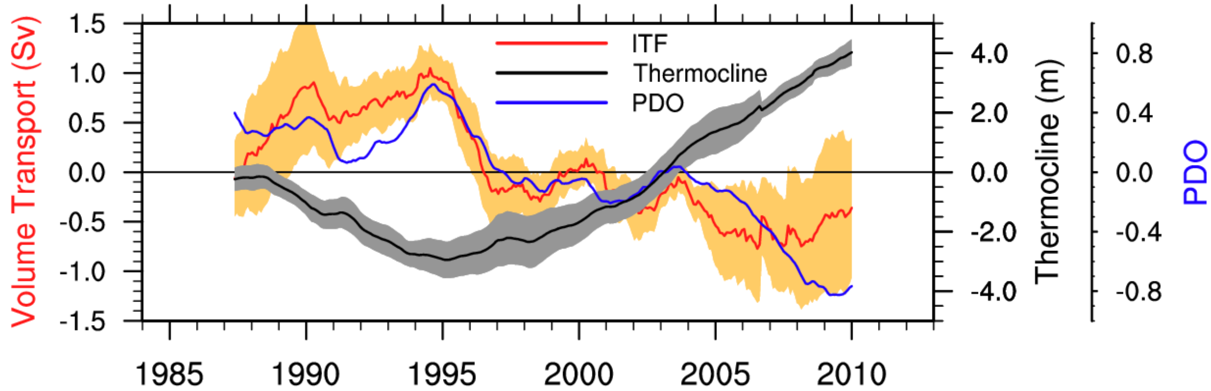

Fig. 9. Time series of 85-month running mean (approximately 7-year to eliminate year-to-year variations) total-depth vertically integrated volume transport by Indonesian Throughflow (ITF) based on the monthly data of four products mean (SODA2.2.4, GECCO2, ORA-S4, ORA-S3; red line), PDO index (blue line), and thermocline depth based on monthly data of seven products mean (Ishii, EN4, GODAS, ORA-S4, SODA2.2.4, ORA-S3, GECCO2) averaged in the southern Indian Ocean (10-40ºS, 40-120ºE; black line). The shading is plus-minus one standard deviation based on all the products used.

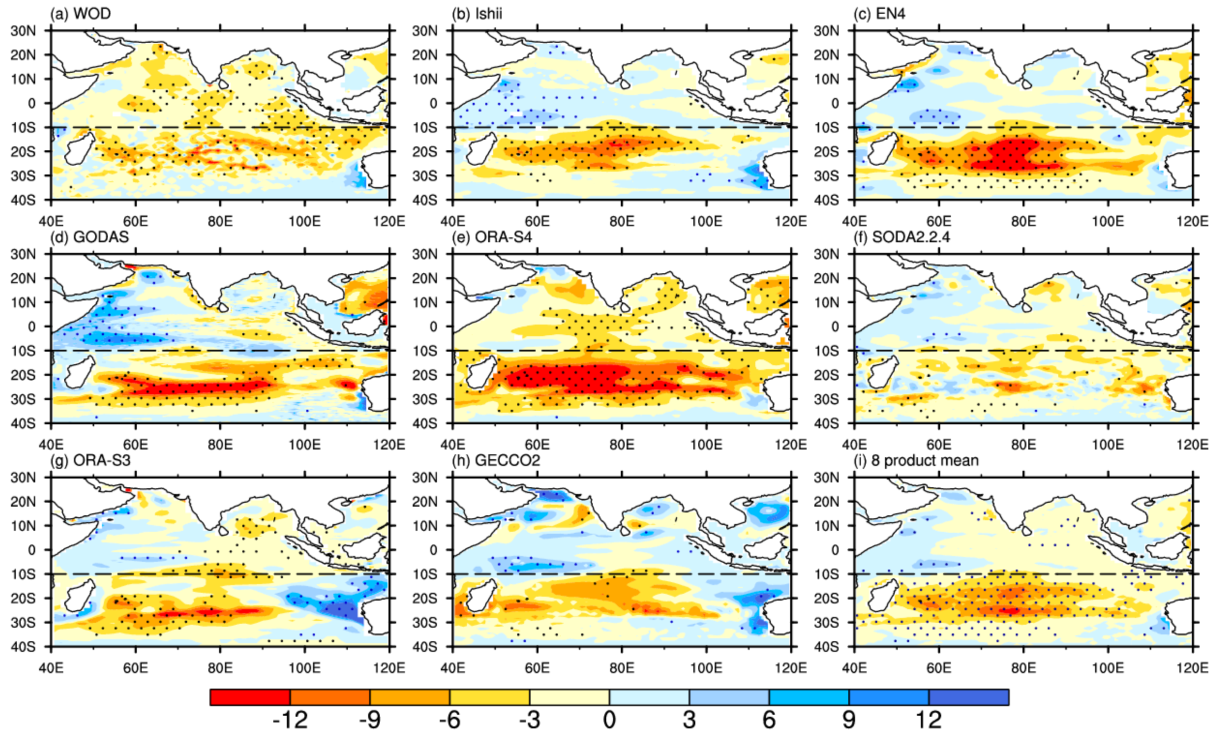

Fig. 10 The regression pattern of 48-month lag thermocline depth onto ITF transport smoothed with an 85-month running mean filter (approximately 7-year to eliminate year-to-year variations) during 1984-2014 from (a) WOD, (b) Ishii, (c) EN4, (d) GODAS, (e) ORA-S4, (f) SODA2.2.4, (g) ORA-S3, (h) GECCO2, (i) eight product mean. Note that the ITF transport used to regress against the data (a-d) is from ORA-S3 as it shows the largest correlation coefficient and closest mean value to INSTANT (Fig. 8), while transports used in (e-h) are based on each product, respectively. To compare with Fig. 6, the color is inverted. Stippling indicates differences that are significantly different from zero with 95% confidence based on a Student t-test. The areal average over the southern Indian Ocean (10-40^{o}S, 40-120^{o}E) regression slope for the 8 product mean is -2.82 m Sv^{-1}. Units: m Sv^{-1}

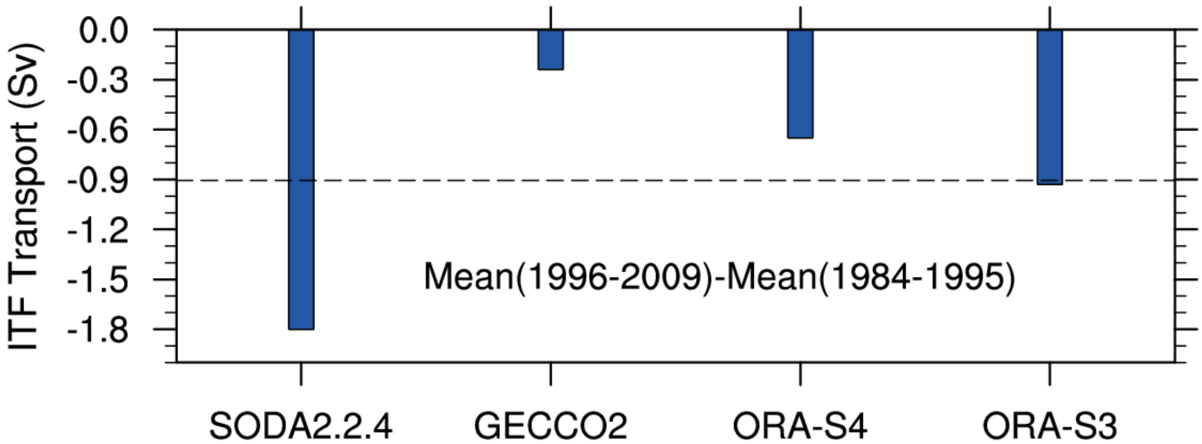

Fig. 11 The differences of mean ITF transport with 4 years earlier than the decades we used for the SST, as the differences between 1996-2009 and 1984-1995 from SODA2.2.4, GECCO2, ORA-S4 and ORA-S3. The dashed line indicates the mean of the four products. Units: Sv = 10^6 m^3 s^{-1}.

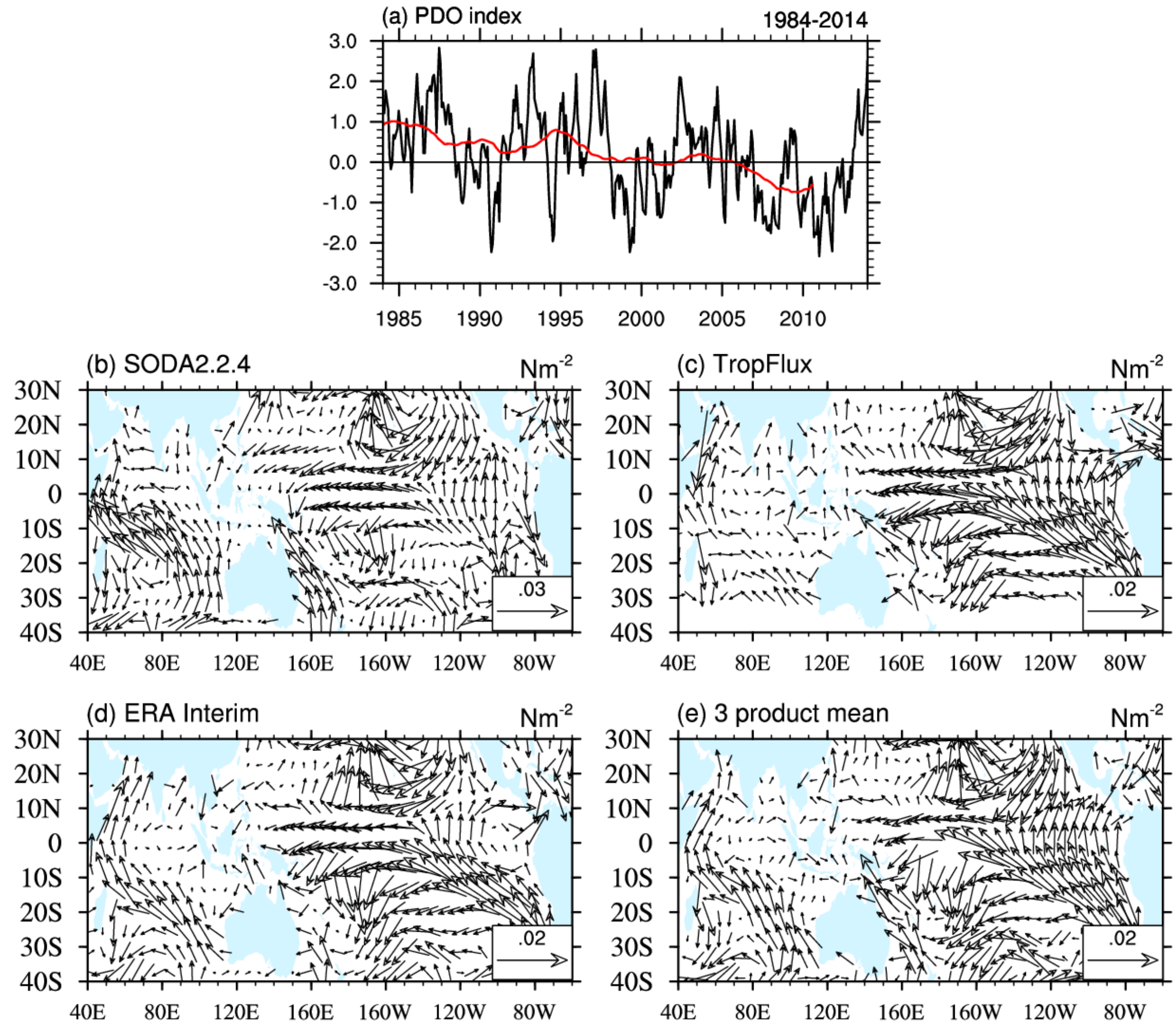

Fig. 12 (a) PDO index during 1984-2014 with monthly values shown as black line and 85-month running mean (approximately 7-year to eliminate year-to-year variations) shown as red line. The regression pattern of surface wind stress onto the 85-month running mean PDO index for (b) SODA2.2.4, (c) TropFlux, (d) ERA Interim and (e) the three product mean. Note that the regression patterns in (b-e) correspond to negative phase of PDO. Units in (b)-(e) are N m^{-2}

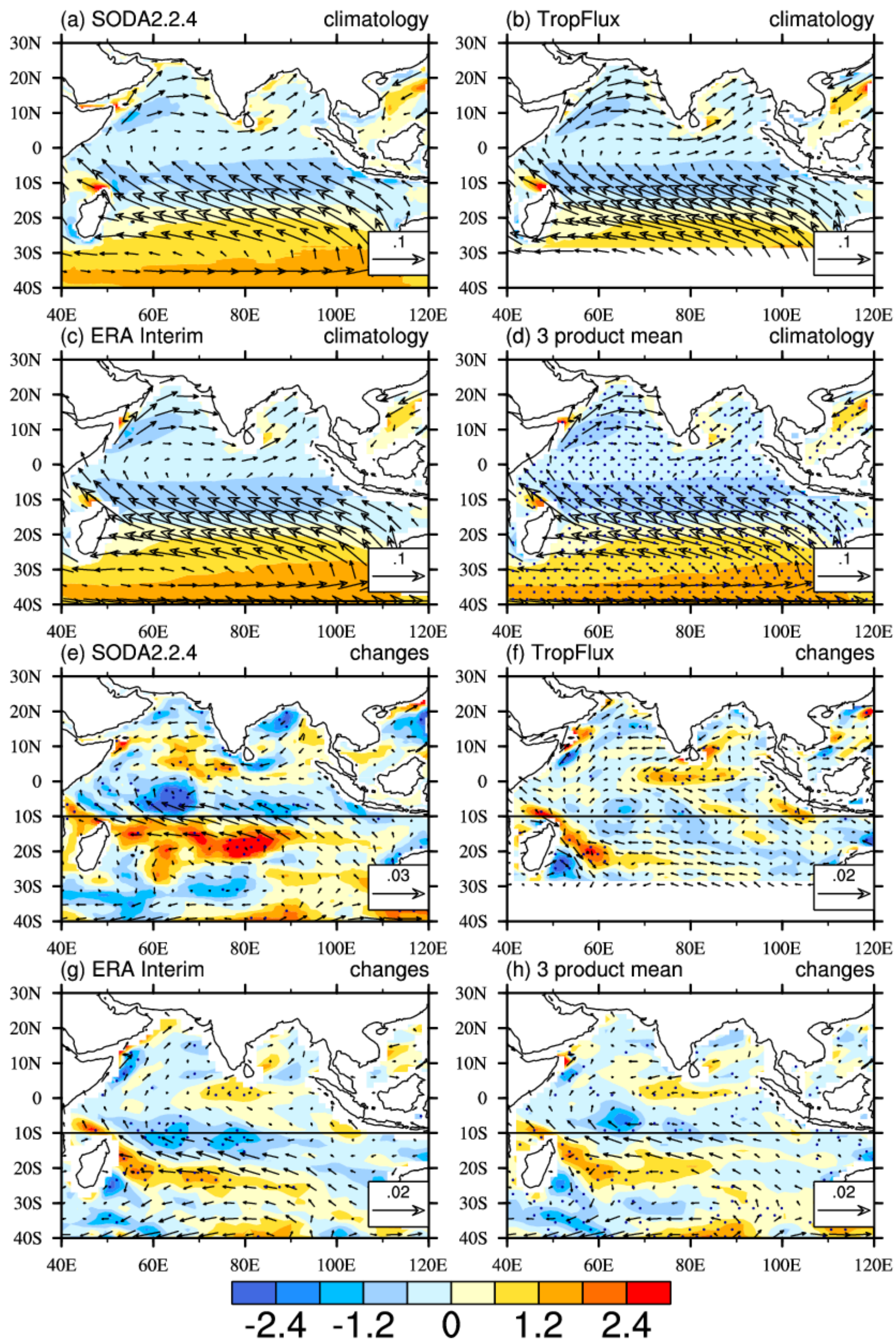

Fig. 13 (a-d) The climatology of surface wind stress (vector, units: N m^{-2}) and its curl (shading, units: 10^{-7} N m^{-3}), (e-h) differences of mean surface wind stress and its curl (units: 10^{-8} N m^{-3}) between the hiatus decade (2000-2013) and pre-hiatus decade (1984-1999) from (a, e) SODA2.2.4, (b, f) TropFlux, (c, g) ERA Interim, (d, h) 3 product mean. Stippling indicates differences that are significantly different from zero with 95% confidence based on a Student t-test.

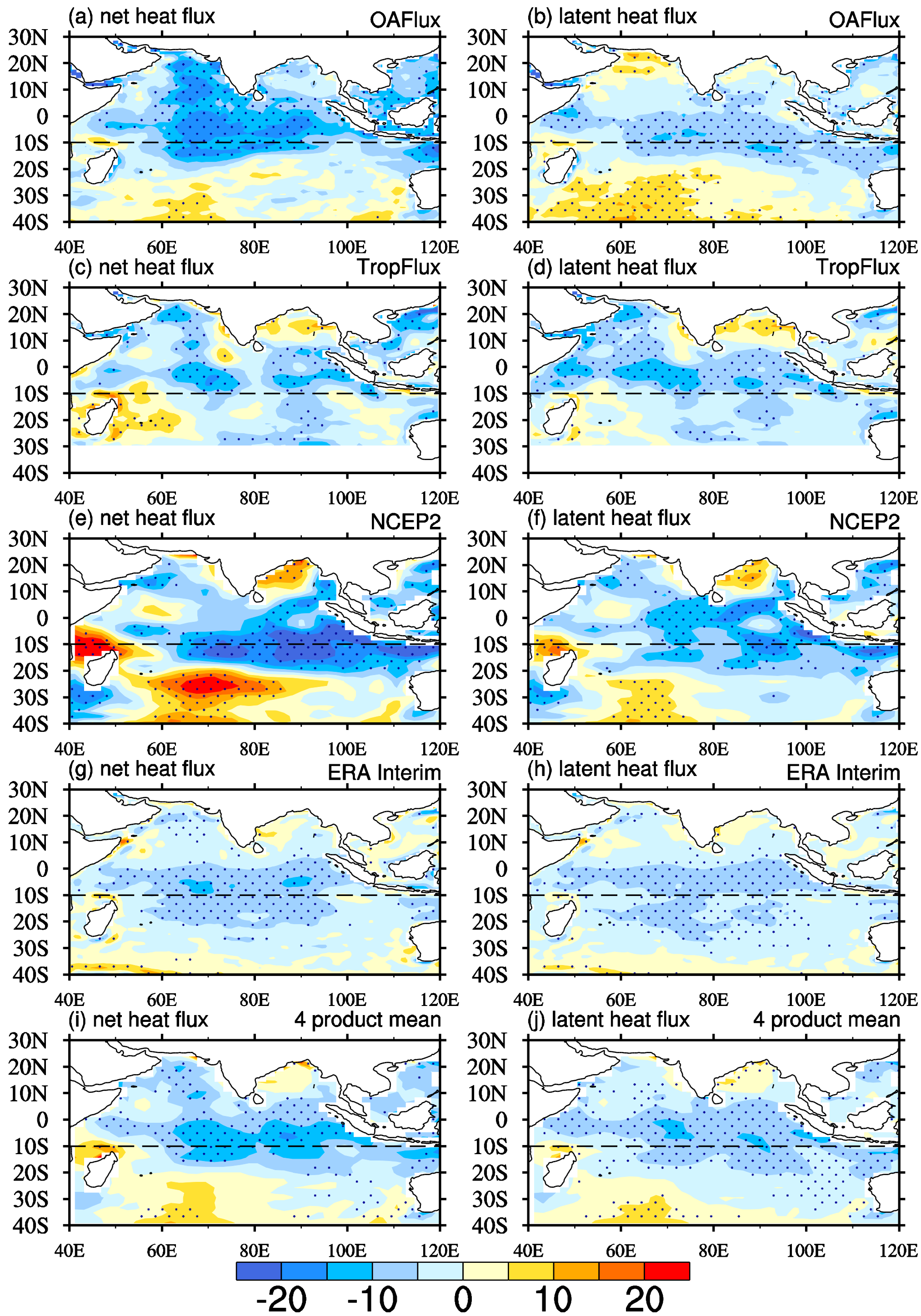

Fig. 14 The differences of mean surface net heat flux (left) and latent heat flux (right) between the hiatus decade (2000-2013) and pre-hiatus decade (1984-1999) from (a, b) OAFlux, (c, d) TropFlux, (e, f) NCEP2, (g, h) ERA Interim, (i, j) four product mean. Setting downward (warming SST) is positive. Stippling indicates differences that are significantly different from zero with 95% confidence based on a Student t-test. Units: W m^{-2}

Figure 1

Click here to access/download

Non-Rendered Figure

Fig.1.eps

Figure 2

Click here to access/download
Non-Rendered Figure
Fig.2.eps

Figure 3

Click here to access/download
Non-Rendered Figure
Fig.3.eps

Figure 4

Click here to access/download
Non-Rendered Figure
Fig.4.eps

Figure 5

Click here to access/download
Non-Rendered Figure
Fig.5.eps

Figure 6

Click here to access/download
Non-Rendered Figure
Fig.6.eps

Figure 7

Click here to access/download
Non-Rendered Figure
Fig.7.eps

Figure 8

Click here to access/download
Non-Rendered Figure
Fig.8.eps

Figure 9

Click here to access/download
Non-Rendered Figure
Fig.9.eps

Figure 10

Click here to access/download
Non-Rendered Figure
Fig.10.eps

Figure 11

Click here to access/download

Non-Rendered Figure

Fig.11.eps

Figure 12

Click here to access/download
Non-Rendered Figure
Fig.12.eps

Figure 13

Click here to access/download
Non-Rendered Figure
Fig.13.eps

Figure 14

Click here to access/download
Non-Rendered Figure
Fig.14.eps